UPPSALA
UNIVERSITET

Digital Comprehensive Summaries of Uppsala Dissertations from the Faculty of Science and Technology 1663

Electronic structure and exchange interactions from ab initio theory

New perspectives and implementations

RAMON CARDIAS ALVES DE ALMEIDA

ACTA
UNIVERSITATIS
UPSALIENSIS
UPPSALA
2018

ISSN 1651-6214
ISBN 978-91-513-0315-4
urn:nbn:se:uu:diva-347812

Dissertation presented at Uppsala University to be publicly examined in Seminar Room, Universidade Federal do Pará, Av. Augusto Correa 01, Belém, PA, Brazil, Belém, Tuesday, 29 May 2018 at 10:00 for the degree of Doctor of Philosophy. The examination will be conducted in English. Faculty examiner: Professor R. B. Muniz (Universidade Federal Fluminense, Instituto de Física, Niterói, RJ, Brazil).

The public defence can also be followed on livestream at Rosetta room, Ång/10239, Ångströmlaboratoriet, Lägerhyddsvägen 1, Uppsala

Abstract
Cardias Alves de Almeida, R. 2018. Electronic structure and exchange interactions from ab initio theory. New perspectives and implementations. *Digital Comprehensive Summaries of Uppsala Dissertations from the Faculty of Science and Technology* 1663. 84 pp. Uppsala: Acta Universitatis Upsaliensis. ISBN 978-91-513-0315-4.

In this thesis, the magnetic properties of several materials were investigated using first principle calculations. The ab initio method named real space linear muffin-tin orbitals atomic sphere approximation (RS-LMTO-ASA) was used to calculate the electronic structure and magnetic properties of bulk systems, surface and nanostructures adsorbed on surfaces.

We have implemented new features in the RS-LMTO-ASA method, such as the calculation of (a) Bloch Spectral Function (BSF), (b) orbital resolved J_{ij} and (c) Dzyaloshinskii-Moriya interaction (DMI). Using (a), we have shown that one can calculate the dispersion relation for bulk systems using a real space method. Furthermore, the dispersion relation was revealed to be existent even for finite one-dimensional structures, such as the Mn chain on Au(111) and Ag(111) surfaces. With (b), we have investigated the orbital resolved exchange coupling parameter J_{ij} for 3*d* metals. It is demonstrated that the nearest neighbor (NN) interaction for bcc Fe has intriguing behavior, however, the contribution coming from the T_{2g} orbitals favours the anti-ferromagnetic coupling behavior. Moreover, the Fermi surface for bcc Fe is formed mostly by the T_{2g} orbitals and these are shown to be highly Heisenberg-like, i.e. do not depend significantly on the magnetic configuration. Later, the same approach was used to study other transition metals, such as Cr, Mn, Co and Ni. In the end, we have presented the results obtained with the implementation (c). Our results have shown the large dependence of the DMI values, both the strength and direction, with respect to which magnetic configuration they are calculated from. We argue that, for the investigated systems, the non-collinearity induces currents (spin and charge) that will influence directly the DMI vectors.

Keywords: ab initio, exchange interactions, non-collinear magnetism

Ramon Cardias Alves de Almeida, Department of Physics and Astronomy, Materials Theory, Box 516, Uppsala University, SE-751 20 Uppsala, Sweden.

ISSN 1651-6214
ISBN 978-91-513-0315-4
urn:nbn:se:uu:diva-347812 (http://urn.kb.se/resolve?urn=urn:nbn:se:uu:diva-347812)

In memory of Corinto Silva de Almeida, my grandfather.

List of papers

This thesis is based on the following papers, which are referred to in the text by their Roman numerals.

I **R. Cardias**, M. M. Bezerra-Neto, M. S. Ribeiro, A. Bergman, A. Szilva, O. Eriksson, and A. B. Klautau.
Magnetic and electronic structure of Mn nanostructures on Ag(111) and Au(111).
Phys. Rev. B **93** 014438 (2016)

II **R. Cardias**, A. Szilva, A. Bergman, I. Di Marco, M. I. Katsnelson, A. I. Lichtenstein, L. Nordström, A. B. Klautau, O. Eriksson and Y. O. Kvashnin.
The Bethe-Slater curve revisited; new insights from electronic structure theory.
Sci. Rep. **7** 4058 (2017)

III Y. O. Kvashnin, **R. Cardias**, A. Szilva, I. Di Marco, M. I. Katsnelson, A. I. Lichtenstein, L. Nordström, A. B. Klautau, and O. Eriksson.
Microscopic Origin of Heisenberg and Non-Heisenberg Exchange Interactions in Ferromagnetic bcc Fe.
Phys. Rev. Lett. **116** 217202 (2016)

IV R. Chimata, E. K. Delczeg-Czirjak, A. Szilva, **R. Cardias**, Y. O. Kvashnin, M. Pereiro, S. Mankovsky, H. Ebert, D. Thonig, B. Sanyal, A. B. Klautau, and O. Eriksson.
Magnetism and ultrafast magnetization dynamics of Co and CoMn alloys at finite temperature.
Phys. Rev. B **95** 214417 (2016)

V A. Szilva, D. Thonig, P. F. Bessarab, Y. O. Kvashnin, D. C. M. Rodrigues, **R. Cardias**, M. Pereiro, L. Nordström, A. Bergman, A. B. Klautau, and O. Eriksson.
Theory of noncollinear interactions beyond Heisenberg exchange: Applications to bcc Fe.
Phys. Rev. B **96** 144413 (2017)

VI **R. Cardias**, M. M. Bezerra-Neto, M. S. Ribeiro, A. Bergman, A. Szilva, Y. O. Kvashnin, L. Nordström, J. Fransson, A. B. Klautau, and O. Eriksson.

First-principles Dzyaloshinskii-Moryia interaction in a non-collinear framework.
In manuscript

Reprints were made with permission from the publishers.

Contents

1. Introduction

Since ancient times, dated centuries B.C., magnetism has been known. Firstly known by its mystic properties, the phenomenon of magnetism has led us to important technological progress. From applications in medical matters to computer storage, magnetism has a fundamental role and its study has been heavily evolving due to the potential future technological applications. Among these new studies, experimental techniques have been widely developed towards the investigation of nanostructures. We can highlight a few, such as (a) Spin-Polarized Scanning Tunneling Microscope (SP-STM) [1–10], which is capable of performing a topological mapping of surfaces on the atomic scale [3–9], provide valuable and precise informations about the magnetic order, differentiate magnetic structures such as collinear or non-collinear [9–11] and investigate the magnetic interactions between the adsorbed nanostructure and the surface [3, 4, 12]; (b) Atomic Force Microscope (AFM) [13], which is a high-resolution type of a scanning probe microscopy (SPM) that provides resolution on the order of fractions of nanometer; (c) X-ray Magnetic Circular Dichroism (XMCD), which is an efficient technique capable to study systems ranging from a single adsorbed atom to surfaces, making it possible to measure the magnetic and orbital moments per atom, as well as the magnetic anisotropy energy (MAE).

In order to understand the electronic and magnetic properties of a given material, one needs to understand how the electrons interact with each other and their environment. This many-body problem is described by the Schrödinger equation. It is an impossible mission to solve it analytically, but one can reformulate the problem with a few approximations. For instance, the Born-Oppenheimer approximation [14, 15], which states that the electrons are assumed to move in the static potential caused by the nuclei, making it possible to decouple the system into separated ionic and electronic problems. By going from a many-body problem to an effective single particle problem, as described and applied in Density Functional Theory (DFT) developed by Hohenberg and Kohn [16, 17], one is able to solve the complexity of the problem.

Through the symbiosis between experimentalists and theoreticians, technology can progress to improve our life. This communication has been more and more challenged by the constant growing complexity of novel materials, for example. With that, constant improvement of well known methods in the literature are needed. There are many different methods that use DFT to calculate the electronic structure of a given system. Particularly here, we have worked to improve the so called real space linear muffin-tin orbitals atomic

sphere approximation (RS-LMTO-ASA) [18–21], which solves the eigenvalue problem in the real space and can also deal with non-collinear magnetism. With the problem being solved in the real space, the study of nanostructures is computationally less costly compared with methods developed in the reciprocal space, such as commonly used methods based on plane waves. It means that one can deal with nanoscaled systems, such as a single atom, islands or nanostructured materials adsorbed on a given surface, without having the symmetry as a problem and where the systems are more likely to present non-collinear magnetism as magnetic ground state. Although DFT methods are designed to be efficient, they are not suitable to describe mesoscopic effects due to their high computational costs. In order to overcome this issue, one can employ multi-scale methods where one can calculate parameters from the DFT, which give the overall behaviour of the system, and use them with Hamiltonians that can model particular problems with higher efficiency. Regarding magnetic systems, one can make use of the spin Hamiltonian to predict important characteristics of a given system, such as the ground state, phase transitions (between phases such as ferromagnetic, anti-ferromagnetic, paramagnetic, skyrmionic phase, etc.), critical temperatures, effect of an external field, the magnetic dynamics, etc. The accuracy of these calculations relies on how well described the system is by a Heisenberg Hamiltonian, or in order words, how much Heisenberg-like is a system. An effective bi-linear spin interaction Hamiltonian can contain three parameters: the exchange coupling parameter J_{ij}, the Dzyaloshinskii-Moryia interaction $\vec{D}_{ij}$ and an anisotropy term. In this thesis, we are going to focus on the two first pair-wise interactions: the exchange coupling parameter J_{ij} and the Dzyaloshinskii-Moryia interaction D_{ij} [22, 23].

Another very usage of the Heisenberg Hamiltonian is to calculate the effective magnetic field experienced by the system and study its spin dynamics properties [24–33]. Particularly, in the information technology sector, efforts are being applied to improve our information exchange speed ratio and our storage power. A new and promising field is the field of spintronics. Spintronics is a broad field and uses the motion of the spin to technological applications. Within this field, one subject has gained a lot of attention lately: skyrmions. Skyrmions, in magnetism, are objects with a topologically protected magnetic configuration with quasiparticle characteristics, which offers possible great applicability in information technology due its mobility and size [34–42]. The study of these materials can be done using a good communication between *ab initio* methods, such as RS-LMTO-ASA, and spin dynamics methods [24–26].

In the present thesis, we have investigated the exchange parameters more carefully by studying closely the elements involved in their calculations. We have implemented new features in the RS-LMTO-ASA method that allow us to study these parameters from new perspectives, which will come to enrich the known knowledge about them and further assist new possibilities of research.

In this way, we present our results in the following chapters. The Chapter 2 will present the many body problem and how DFT approaches this. Moreover, it will be shown how the RS-LMTO-ASA method uses DFT to calculate the electronic structure of metals. The Chapter 3 is focused in the investigation done with respect to the exchange parameters. We show our implementations and new contributions to the RS-LMTO-ASA method. In Chapter 4 we give a small brief about our papers and lastly we present an outlook of the thesis, followed by the Appendixes A, B and C with a brief description of the theoretical background.

2. Density Functional Theory (DFT)

2.1 The many body problem

Many of the physical properties of materials can be studied if the behavior of electrons is known. Therefore, electronic structure calculation of solids is one of the most important methods to understand these properties. Moreover, the theoretical study of electronic structure, in general, helps to understand better the phenomena observed experimentally and to predict phenomena that are not yet observed.

In order to complete this task, one should calculate the eigenstates for an interacting multi-electronic system. That means that one needs to find the solution for the Schrödinger, written as:

$$\hat{H}\psi_j(\vec{r}) = E\psi_j(\vec{r}), \tag{2.1}$$

where E is the total energy of the system and $\hat{H}$ is the Hamiltonian operator, which in this case is described, in Rydberg units, by:

$$\hat{H} = -\sum_i \frac{\nabla^2_{R_i}}{M_i} + \sum_{i\neq j} \frac{Z_i Z_j}{|\vec{R}_i - \vec{R}_j|} - \sum_i \nabla^2_{r_i} + \sum_{i\neq j} \frac{1}{|\vec{r}_i - \vec{r}_j|} - \sum_{i,j} \frac{2Z_i}{|\vec{r}_i - \vec{R}_j|}, \tag{2.2}$$

where $\vec{R}$ and $\vec{r}$ are the coordinates for each nuclei and electron, respectively. Z is the atomic number of each atom and M is the mass of each nuclei. The Hamiltonian is composed by kinetic operators of the nuclei and electrons, first and third terms respectively. The second, fourth and fifth terms are the Coulomb interactions nuclei-nuclei, electron-electron and electron-nuclei; respectively. In our case, for solids, this is an impossible problem to solve due to the amount of particles to be taken in consideration. Therefore, one should be careful and use the appropriate approximation to overcome the many body problem, in order to give reliable results.

A good approximation for the problems we are interested in is the so called Born-Oppenheimer approximation, or adiabatic approximation, which states that the nuclei are much heavier than the electrons and, therefore, the electron response for any nuclei movement is given in a very small interval of time. This allows us to consider the nuclei with a fixed position with respect to the electron position, enabling to study the nuclei and electrons independently.

With the Born-Oppenheimer approximation, we reduce the problem to a calculation of stationary states of a system of electrons moving influenced by

an electrostatic field generated by the fixed nuclei. Although this approximation simplifies the Hamiltonian, the electron-electron interaction is still a complicated many body problem. Consequently, further approximations are needed to solve the problem.

2.2 Introduction to DFT

One way of reformulate the problem is to go from a many body problem to many problems of a single body. Under the light of this thinking, Hohenberg, Kohn and Sham developed the so called Density Functional Theory (DFT) [16, 17]. The theory uses the electronic density of the ground state $\eta_0(\vec{r})$ as its main variable. From that new variable, one can then calculate the properties, such as the magnetic properties of the system, which is the aim of this work. The theory is sustained by two fundamental theorems:

1. The external potential, V_{ext}, where the electrons are immersed, is a unique functional of the electronic density $\eta(\vec{r})$.
2. The energy functional $E[\eta]$ is minimized by the electronic the ground state density $\eta_0(\vec{r})$.

As a consequence of these theorems, Kohn and Sham [43] demonstrated that instead of solving the Schrödinger equation for the many body problem, one can solve the problem of one electron that moves subjected by an effective field described by electrostatic terms and one quantum term known as exchange-correlation interaction. The equation that describes that problem is known as the Kohn-Sham equation:

$$[-\nabla^2 + V_{ef}(\vec{r})]\psi_i(\vec{r}) = \varepsilon_i \psi_i(\vec{r}). \tag{2.3}$$

The Eqn. 2.3 is a *Schrödinger-like* equation, where now the effective potential V_{ef} is a function of the electronic density $\eta(\vec{r})$, and is described by

$$V_{ef} = V_{ext} + 2\int \frac{\eta(\vec{r'})}{|\vec{r} - \vec{r'}|} d\vec{r'} + V_{xc}(\eta(\vec{r})). \tag{2.4}$$

In the Eqn. 2.4, V_{ext} represents the external potential due the atomic nuclei, V_{xc} stands for the exchange-correlation potential and the central term is the electrostatic potential between the electrons, commonly known as the Hartree term.

With the Eqns. 2.3 and 2.4, it is possible to calculate the wave function $\psi_i(\vec{r})$ and the energy ε_i of each electron of the studied atom. Note that the effective potential V_{ef} is a function of the electronic density $\eta(\vec{r})$, which is determined by $\eta(\vec{r}) = \sum_i |\psi_i|^2$. That means that the calculation must be done in an iterative fashion. In general, one guess an initial value for the electronic density and then the external potential is calculated to solve the Kohn-Sham equation in order to obtain the wave functions. From the wave functions, a

new electronic density is calculated, which is then typically mixed with the old electronic density. The resulting electronic density is used again to give continuity to the self-consistent process. This process is maintained until the resulting electronic density is the same as the input electronic density, given a certain convergence limit.

Now, one more part of the problem needs do be treated: the exchange-correlation V_{xc}. Since the exchange-correlation is not known for real materials, one needs to use an appropriate approximation. Since we are dealing with metallic systems, it is reliable to treat the system as an interacting homogeneous electron gas. This approximation is called Local Density Approximation and will be further discussed in the next section.

2.3 Local Density Approximation

Now, the problem to be solved is on finding the adequate approximation for the exchange-correlation term. Kohn and Sham [43] proposed an approximation which consists in taking a non-homogeneous system of many electrons and consider it as small subsystems of a homogeneous interacting electron gas. This approximation is called Local Density Approximation (LDA). In this approximation, it is assumed that the electronic density $\eta(\vec{r})$ varies smoothly around a given point in space $\vec{r}$, thus, the exchange-correlation energy is defined as an integration over all space, where the exchange-correlation energy density is the same as the homogeneous electron gas. In this way, one can write the exchange-correlation energy as follows

$$E_{xc}[\eta] = \int \eta(\vec{r})\varepsilon_{xc}(\eta(\vec{r}))d\vec{r}, \tag{2.5}$$

where ε_{xc} is the exchange-correlation energy per electron. Therefore, one can write the exchange-correlation potential V_{xc} as

$$V_{xc}[\eta] = \frac{d}{d\eta(\vec{r})}\left\{\eta(\vec{r})\varepsilon_{xc}(\eta(\vec{r}))\right\}. \tag{2.6}$$

If one is dealing with spin polarized systems, it is possible to extend the Local Density Approximation to Local Spin Density Approximation (LSDA). In this case, the magnetization density is described by the difference between the majority band $\eta^{\uparrow}(\vec{r})$ and minority bands $\eta^{\downarrow}(\vec{r})$. The new spin dependent exchange-correlation energy is now written as

$$E_{xc}[\eta] = \int \eta(\vec{r})\varepsilon_{xc}(\eta^{\uparrow}(\vec{r}),\eta^{\downarrow}(\vec{r}))d\vec{r}. \tag{2.7}$$

With the new spin dependent exchange-correlation potential V_{xc} as

$$V_{xc}^{k} = \frac{\partial}{\partial n^{k}}\{\eta(\vec{r})\varepsilon_{xc}(\eta^{\uparrow}(\vec{r}),\eta^{\downarrow}(\vec{r}))\}, \tag{2.8}$$

where the index k can be either $\uparrow$ or $\downarrow$. It is still possible to parametrize the exchange-correlation energy by parametrizing the term ε_{xc} in order to facilitate the obtaining of the exchange-correlation potential. Here, we will make use of the Barth-Hedin parametrization [44].

2.4 Spin polarized systems

In the case of spin-polarized systems, it is convenient to substitute the electronic density $\eta(\vec{r})$ by a electronic density matrix $\rho(\vec{r})$, described by

$$\eta(\vec{r}) \Rightarrow \rho(\vec{r}) = \frac{\eta(\vec{r})}{2}\mathbf{1} + \frac{\vec{m}(\vec{r})}{2}\sigma, \tag{2.9}$$

where $\vec{m}(\vec{r})$ is the magnetization density, σ are the Pauli matrices and $\mathbf{1}$ is a 2x2 unitary matrix. The wave functions are now described with spinors:

$$\psi_i(\vec{r}) = \begin{bmatrix} \alpha_i(\vec{r}) \\ \beta_i(\vec{r}) \end{bmatrix}, \tag{2.10}$$

where α_i and β_i are the spin projections. The electronic density matrix is now expressed as a function of the spinors as

$$\rho(\vec{r}) = \sum_{i=1}^{N} \begin{bmatrix} |\alpha_i(\vec{r})|^2 & \alpha_i(\vec{r})\beta_i(\vec{r})^* \\ \alpha_i(\vec{r})^*\beta_i(\vec{r}) & |\beta_i(\vec{r})|^2 \end{bmatrix}. \tag{2.11}$$

Now, one can write the magnetization density $\vec{m}(\vec{r})$ and the charge density $\eta(\vec{r})$ as

$$\vec{m}(\vec{r}) = \sum_{i=1}^{N} \psi_i(\vec{r})^{\dagger}\sigma\psi_i(\vec{r}), \tag{2.12}$$

$$\eta(\vec{r}) = Tr(\rho(\vec{r})) = \sum_{i=1}^{N} |\psi_i(\vec{r})|^2, \tag{2.13}$$

where N is the number of states in the system. Analogous to the density matrix, the external potential can also be extended to a 2x2 matrix. Thus, the non-magnetic Eqn. 2.3 can be generalized in the following way

$$(-\nabla^2 + V_{ef}^{\sigma}(\vec{r}))\psi_i^{\sigma}(\vec{r}) = \varepsilon_i^{\sigma}\psi_i^{\sigma}(\vec{r}). \tag{2.14}$$

Now, one is able to split the effective potential in a magnetic term, $\mathbf{b}$, and a non-magnetic term, V_{nm}. In this way, the Kohn-Sham Hamiltonian for a spin-polarized system can be written as

$$H = (-\nabla^2 + V_{nm})\mathbf{1} + \mathbf{b}\cdot\sigma. \tag{2.15}$$

The non-magnetic part of the Hamiltonian is diagonal and if the system is collinear, i.e. system has a global magnetization axis, the spin dependent term can also be obtained in the diagonal form. Once the Hamiltonian is diagonal, the spin projections do not hybridize with each other (if the spin-orbit coupling is neglected), enabling the problem to be solved independently. When this case is not possible, i.e. there is not a global magnetization axis, then we have a non-collinear magnetism case. This particular case will be analysed further in this thesis.

2.5 Spin-orbit coupling

The Hamiltonian described by the Eqn. 2.15 takes into consideration only scalar relativistic effects. However, to be able to have a more accurate description, when the fully relativistic effects become important, one needs to include the spin-orbit coupling effect. This can be done solving the Dirac equation for the spin-polarized systems or one can add the spin-orbit coupling to the scalar relativistic Hamiltonian as a perturbation [45–47], updated at every self-consistent step. Thus, the new Hamiltonian is written as

$$H = H_{SR} + \xi \mathbf{L} \cdot \mathbf{S}, \tag{2.16}$$

where the H_{SR} is the scalar relativistic Hamiltonian and ξ is the spin-orbit coupling parameter. The latter is described as

$$\xi \propto \frac{1}{r} \frac{\partial V}{\partial r}, \tag{2.17}$$

which is influenced by the atomic number, therefore, the spin-orbit effects are stronger for heavy elements [48, 49].

2.6 The RS-LMTO-ASA method

2.6.1 Introduction

It is known that the Eqn. 2.3 needs to be solved in a self-consistent method. The Real Space - Linear Muffin-Tin Orbital - Atomic Sphere Approximation (RS-LMTO-ASA) [18] is self-consistent, DFT based method, applied in the real space, based on the LMTO-ASA formalism (Appendix A) and uses the recursion method (Appendix B). The advantage of having a method developed in the real space is that one can study systems without any periodicity, i.e. does not rely in symmetry restrictions. That makes it an appropriate method to deal with metallic alloys, defects on surfaces, interstitial impurities, etc [19–21]. The RS-LMTO-ASA method is a linear method with which the solutions are more precise around a given energy E_v, usually taken as the gravity center of the occupied bands s, p and d [45].

The method works in the orthogonal representation of the LMTO-ASA formalism, nevertheless, the orthogonal Hamiltonian is expanded in terms of tight-binding parameters (TB) [50] for the better use of the recursion method. Here, we use the upper bar to represent the tight-binding basis. Thus, the Hamiltonian in the orthogonal basis written in terms of parameters from TB representation is given as

$$H = E_v + \bar{h}(1+\bar{o}\bar{h})^{-1}. \tag{2.18}$$

If $\bar{o}\bar{h}$ is too small, one can expand the $(1+\bar{o}\bar{h})^{-1}$ in a series of $\bar{o}\bar{h}$, thus obtaining

$$H = E_v + \bar{h} - \bar{h}\bar{o}\bar{h} + \bar{h}\bar{o}\bar{h}\bar{o}\bar{h} - \cdots, \tag{2.19}$$

where $\bar{h}$ is a Hermitian matrix expressed as a function of the TB terms (see Appendix A), described by

$$\bar{h} = \bar{C} - E_v + \bar{\Delta}^{\frac{1}{2}}\bar{S}\bar{\Delta}^{\frac{1}{2}}. \tag{2.20}$$

In this case, one can use the Hamiltonian in its first order approximation

$$H = H^{(1)} = E_v + \bar{h} \tag{2.21}$$

or in its second order

$$H = H^{(2)} = H^{(1)} - \bar{h}\bar{o}\bar{h}. \tag{2.22}$$

In our case, to describe the occupied part of the bands s, p and d, the first order approximation is typically enough. The second order approximation is useful when the unoccupied part of these bands are important. Therefore, the Hamiltonian with the first order approximation is given by

$$H = \bar{C} + \bar{\Delta}^{\frac{1}{2}}\bar{S}\bar{\Delta}^{\frac{1}{2}}. \tag{2.23}$$

Here, $\bar{C}$ and $\bar{\Delta}$ are potential parameters related to the calculation of the Eqn. 2.3 in each sphere and represent, respectively, the center and the width of the density of state from site R. The structure matrix $\bar{S}$ is a part of the Hamiltonian independent of the potential at site R, V_R. From the Eqn. 2.23, one needs to solve the eigenvalue problem, which can be solved in the real space using the recursion method (see Appendix B):

$$(H-E)u = 0, \tag{2.24}$$

where H is the considered Hamiltonian, E is the eigenvalue and u the eigenvector. Taking the expansion around a fixed and arbitrary energy $E = E_v$ for ψ, we have

$$\psi(r,E) = \sum_{RL}[\varphi_{lv}(r_R) + (E-E_v)\dot{\varphi}_{lv}(r_R)]\,Y_L(\hat{r}_R). \tag{2.25}$$

The functions $\varphi_{lv}(r_R)$ and $\dot{\varphi}_{lv}(r_R)$ are the solutions of the Eqn. 2.3, indexed by the quantum numbers $L = (l,m)$, and its first derivative with respect to energy, calculated in E_v. These functions are defined inside the Wigner-Seitz (WS) sphere of the site R and zero outside this region.

Now, in the next section, we will focus on the self-consistent process, as well as the difference between the process done for the two-dimensional (2D) metallic systems and for the defects in these 2D systems.

2.6.2 Generalized self consistent process in the RS-LMTO-ASA

The process used in the RS-LMTO-ASA method consists in two different linked processes: an atomic and a main part. In the former process, the parameters are found by solving the Kohn-Sham equation inside the muffin-tin spheres (MT), which is solved for every non-equivalent site. The equivalent spheres are the one with the same potential parameters and, thus, have the same occupation, local density of states, etc.

Main part

Before describing the process, keep in mind a few observations related to the basis choice, which can be found in the Appendix A with a more detailed description. According to Andersen *et al.* [51], the LMTO-ASA formalism gives us the possibility of different basis choices $\{\chi_i\}$ for the expansion of the wave function described in Eqn. 2.25. That means that one can choose the more convenient basis more suitable for each particular case. Originally, this formalism was developed in the canonical basis, however, for the systems studied in this thesis, two other bases will be used that simplify our calculations. One of the basis will be used with which the functions are orthogonal between themselves, which simplifies the eigenvalue problem. The second is the tight-binding basis (TB), to simplify the recursion method. From the canonic basis, the other basis can be described in terms of mixture terms, denoted by Q. Here, the upper bar still represents the TB basis, but the variables with no superscripts are the variables in orthogonal basis. The relation between the orthogonal basis and the TB basis can be written as the following:

$$\frac{\Delta^{\frac{1}{2}}}{\bar{\Delta}^{\frac{1}{2}}} = 1 - (\bar{Q} - Q)\frac{\bar{C} - E_v}{\bar{\Delta}} = \frac{C - E_v}{\bar{C} - E_v}. \tag{2.26}$$

For the TB basis, the parameters $\bar{Q}$ are constant and independent of the material. In this way, it is now possible to split the problem in two parts. The first one is structure-related only and has the objective to calculate the structure constant matrix $\bar{S}$ of the Hamiltonian described in the Eqn. 2.23, responsible for connecting several sites.

$$\bar{S} = S^0(\mathbf{1} - \bar{Q}S^0)^{-1}, \tag{2.27}$$

where $\mathbf{1}$ is the identity matrix and S^0 is the structure constant in the canonic basis, which values can be found in the literature [51]. Note that in our calculations, $\bar{S}$ is constant and is calculated only once.

Once the structure matrix is calculated, the next step is to calculate the other potential TB parameters $\bar{C}$ and $\bar{\Delta}$, which are related with the center of the band and the band width (in the TB basis), respectively. So, the process consist in guessing initial values for the $\bar{C}$ and $\bar{\Delta}$ (calculated within the atomic part), the Hamiltonian 2.23 is constructed, and the eigenvalue problem is solved by Eqn. 2.24 and lastly the density of states per spin (LDOS) is calculated for each of the non-equivalent sites and for each orbital L $(L = l,m)$, denoted by $N_{RL}(E)$. The latter step is done by using the recursion method [52] and the Beer-Perttifor terminator [53] (see Appendix B). It is noteworthy to say that this method is efficient only if one has a sparse Hamiltonian, i.e. with a lot of zeros, and that is why the TB basis is chosen here.

Once the $N_{RL}(E)$ are calculated, it is possible to obtain the moments, $m_{Rl}^{(q)}$, of order "q"$(q = 0,1,2)$ of the LDOS, for a given energy E_v, using the following equation:

$$m_{Rl}^{(q)} = \int_{-\infty}^{E_F} (E - E_v)^q N_{Rl}(E) dE. \tag{2.28}$$

As commented earlier, E_v is chosen as the gravity center of the occupied band. Consequently, in this region, the moment $m_{Rl}^{(1)}$ is zero, whereas the moment $m_{Rl}^{(0)}$ gives the occupation of each orbital. After the moments are calculated, the next step is to calculate the potential parameters $P_l(l = 0,1,2)$. We define P_l as

$$P_l = 0.5 - \frac{1}{\pi} arctg(D_l), \tag{2.29}$$

where D_l is the logarithm derivative of the Eqn. 2.3 with respect to a given orbital l calculated in the sphere boundary. D_l can be described as

$$D_l = 1 + (2l+1)\left[\frac{Q_l^{-1}}{2(2l+1)} \frac{C_l - E_v}{C_l - E_v - \Delta Q_l^{-1}} - 1\right]. \tag{2.30}$$

Once these parameters are calculated, one can start the atomic part of the procedure. In this step, we calculate self-consistently the potential parameters at each non-equivalent site in order to determine the new C, Δ and Q.

Together with the atomic part, the Madelung potential V_{mad} is calculated (see more details next in Eqn. 2.37), which gives us the energy due the fact that the sites are inserted in a crystal and, therefore, there are charge transfer between them. In essence, this is the electrostatic potential of the electrons

within the crystal and has the job to adjust the values in the center of the band and E_v.

With the new C, Δ, Q and V_{mad}, the relation between the orthogonal basis and the TB basis is used, Eqn. 2.26, to obtain the new values for $\bar{C}$, $\bar{\Delta}$ and $\bar{Q}$. This process is done self-consistently until the convergence is reached. In Fig. 2.1, it is shown schematically how the main part of the RS-LMTO-ASA method calculation is done.

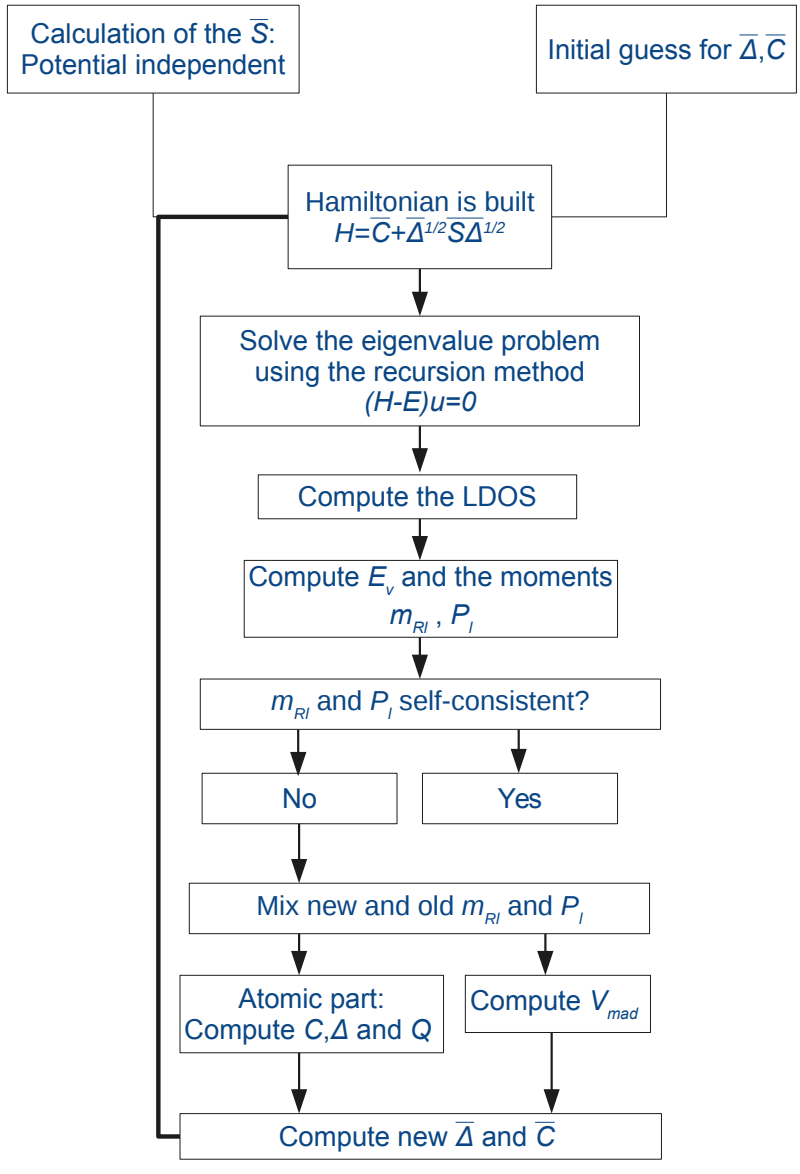

Figure 2.1. Self-consistent process of the RS-LMTO-ASA method - General Part.

Atomic part

In this self-consistent step, the objective is to find the potential and the potential parameters for each non-equivalent sphere of the crystal, using the conditions established by the found values for $m_{Rl}^{(q)}$ and P_l, Eqns. 2.28 and 2.29, respectively. It is done by solving the Eqn. 2.3 inside of each sphere, evaluating then the potential and the potential parameters defined in the orthogonal basis (C_{Rl}, Δ_{Rl} and Q_{Rl}).

Now, an initial estimative is given for φ_{Rl}, for the three first moments of the density of states $m_{Rl}^{n}(m_{Rl}^{(0)}, m_{Rl}^{(1)} = 0, m_{Rl}^{(2)})$ and for the parameter P_l. From there, the electronic density $\eta_R(r)$ of each non-equivalent sphere centred in the site R is obtained, given by equation

$$\eta_{Rl}(r_R) = \frac{1}{4\pi} \sum_l \left[m_{Rl}^{(0)} \varphi_{Rl}^2 + m_{Rl}^{(2)} (\dot{\varphi}_{Rl}^2 + \varphi_{Rl} \ddot{\varphi}_{Rl}) \right], \tag{2.31}$$

where $\dot{\varphi}_{Rl}$ and $\ddot{\varphi}_{Rl}$ are, respectively, the first and the second derivative with respect to the energy of the Eqn. 2.3 radial solution, inside the sphere with radius R and both calculated for the energy E_v. With the electronic density calculated, it is now possible to calculate the electrostatic potential V_E using the Poisson equation, defined, in atomic units (Rydberg), by

$$\nabla^2 V_E(r) = -8\pi \eta_{Rl}(r). \tag{2.32}$$

To this potential, the contribution coming from the electrostatic potential of the studied atom, V_N, is added. The contribution coming from the exchange-correlation potential V_{xc}, obtained with the LSDA approximation is then also added. With these new contributions, the new potential can be written as

$$V_R = V_E(\eta_{Rl}(r)) + V_{xc}(\eta_{Rl}(r)) + V_N, \tag{2.33}$$

where V_N is given by

$$V_N = -\frac{2Z}{r}. \tag{2.34}$$

With the new potential and the boundary conditions determined by P_l, one can obtain the new wave functions solving the Eqn. 2.3 centred in the sphere of radius R, for a given energy $E_{v,Rl}$

$$(-\nabla^2 + V_R)\varphi_{Rl}(r) = E_{v,Rl} \varphi_{Rl}(r). \tag{2.35}$$

When the new wave functions φ_{Rl} and their derivatives are known, one can calculate a new electronic density, Eqn. 2.31, $\eta_{Rl}(r)$. It is then verified if the calculation is converged, which is done by checking if the output value for the density is inside a given convergence range compared with the old electronic density. If this condition is not met, i.e. convergence is not satisfied, a mixing

in terms of weighted average is done between the input and output values for the density, weighted by a value β

$$\eta_{Rl}(r) = \beta \eta_{Rl}^{new}(r) + (1-\beta)\eta_{Rl}^{old}(r), \tag{2.36}$$

where β is a parameter with values $0 \leq \beta \leq 1$. The result obtained from this weighted is then used for a new self-consistent procedure with all the steps before explained, until the convergence is met.

Once the convergence is reached, the converged wave functions $\varphi_{Rl}(r)$ are obtained. With $\varphi_{Rl}(r)$, its derivatives and the boundary conditions P_l, the new potential parameters C_{Rl}, Δ_{Rl} and Q_{Rl} are calculated, in orthogonal basis.

Note that in Eqn. 2.33, the potential due other spheres is not taken in consideration. Due to that, a correction is needed in order to considers the charge distribution of the calculated sphere's neighbors and the electronic contribution of the calculated sphere itself. This correction is given by the Madelung potential, described by

$$V_{mad}^{i} = \sum_{j \neq i} \frac{2TDQ(j)}{|\vec{R}_i - \vec{R}_j|} + \frac{2TDQ(i)}{R_{WS}}, \tag{2.37}$$

where R_i is the position of the reference sphere, $|\vec{R}_i - \vec{R}_j|$ the distance between the site i and j, R_{WS} the Wigner-Seitz radius and TDQ the relative charge transference of site i. The first term is the reference sphere potential generated by the Coulomb interaction with the neighbor spheres (off-site contribution), whereas the second term is the potential of the reference sphere itself (on-site contribution).

As already mentioned before, the Madelung potential V_{mad} shifts the energy scale, shifting E_v to $E_v + V_{mad}$ and the parameter C to $C + V_{mad}$. The scheme of the explained procedure is shown in Fig. 2.2.

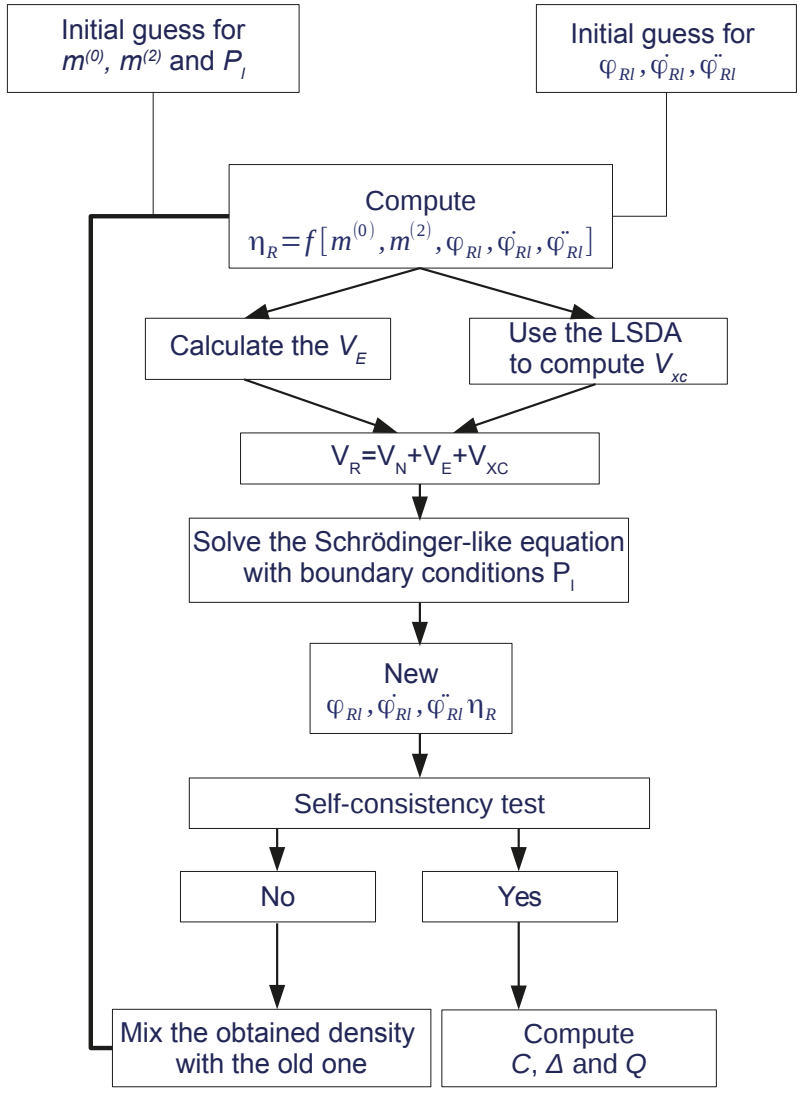

Figure 2.2. Self-consistent process of the RS-LMTO-ASA - Atomic Part.

2.6.3 Self consistent process for metallic surfaces

The RS-LMTO-ASA self-consistent method explained in the previous section can be applied for any metallic system, however, the electrostatic potential V_E and the Fermi energy E_F must be calculated according to the studied system. In this section, we describe the process to obtain these values for metallic surfaces.

To study metallic surfaces using the RS-LMTO-ASA method, the semi-infinite structure of the metallic system is simulated by a large cluster with several thousands of atoms positioned in atomic planes parallel to the crystal plane of the surface which is being calculated (e.g [001], [110], [111]). It is known that a small amount of charge can be transferred to regions outside of the Wigner-Seitz sphere of the atoms in the surface. To compensate this effect, one or two empty sphere layers are included to simulate the vacuum. Therefore, it is possible to calculate the amount of charge in the surface neighborhood. With the charge being transferred to the empty sphere layer, the surface will be positively charged whereas the empty sphere layer will be negatively charged. That characterizes a parallel plates capacitor, which will change the electrostatic potential in sites far away sites from the surface and this shifts the Fermi energy from a value that depends on the transferred sites around the surface [54, 55]. In order to avoid this Fermi energy shifting, a new energy scale is defined where the potential felt from far away sites is null. Therefore, for any two-dimensional/surface calculation, the Fermi energy is fixed to the value found self-consistently for the bulk system.

The Fermi energy E_F for the bulk material can be calculated using the following equation:

$$\sum_{RL} \int^{E_F} N_{RL}(E) dE = Q_V, \tag{2.38}$$

where Q_V is the valence charge. Once the Fermi energy E_F is fixed, it is possible to calculate the local density of states (LDOS) and determinate the charge transfer in each site, including the empty spheres.

For periodic crystals, the electrostatic potential V_E is obtained using the Ewald summation, where all the multipole potential contribution plus the charge in each sphere are considered. However, the case of a surface is more complicated. Here, the symmetry holds only along the planes parallel to the surface and each surface has its own electrostatic potential. For this case, the two-dimensional Ewald summation by Skriver *et al* [54, 55] is used, in order to obtain the electrostatic potential V_E and the Madelung potential V_{mad} for each site.

Physically, it is expected that layers far away from the surface will not feel the effects due the surface, therefore, the parameters Δ and C for these far away layers will be the same as the bulk parameters. In this way, only layers close to the surface are treated self-consistently. So, for the self-consistent calculation,

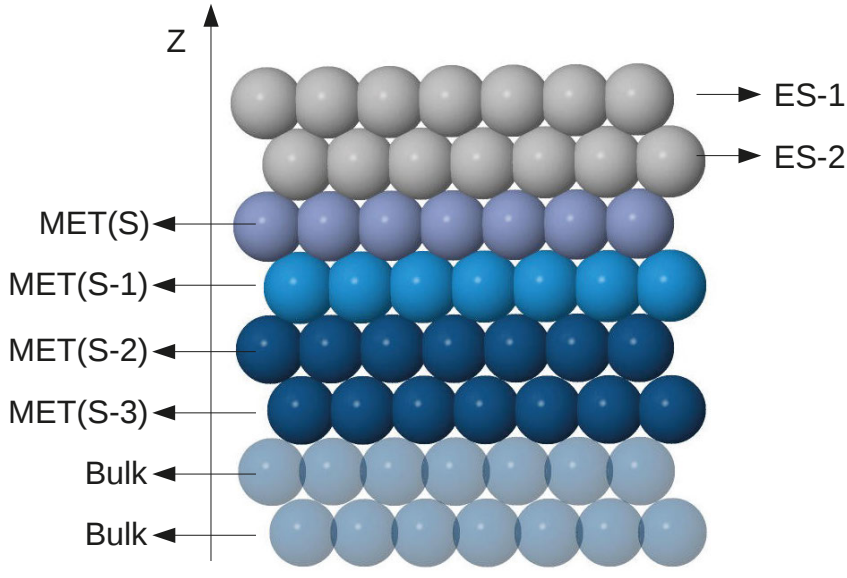

Figure 2.3. Schematic representation of the generic surface, without including the defect, such as an embedded or adsorbed atom.

a certain number of empty sphere layers are included (usually one or two), which will simulate the vacuum (ES-2, ES-1; Fig. 2.3), and a number n of metallic layers (Met(S-1), Met(S-2), Met(S-3)) under the surface (Met(S)). The number of layers n are chosen in a way that all the considered layers in the self-consistent procedure have different parameters compared with the bulk system.

2.6.4 Self consistent process for an isolated defect on metallic surfaces

In order to study the effects due to isolated defects, impurities, nanostructured systems, etc; using the RS-LMTO-ASA, one should initially have the surface converged, following the scheme outlined in Sec. 2.6.3. Once the surface is converged, the desired system can be calculated. For the impurity calculation, the Fermi energy is fixed to the bulk value, i.e. E_F is not updated at every iteration. The electrostatic potential, charge transfer and potential parameters are also fixed for the sites far away from the defect, which it is considered to not be affected by the impurity.

Once the defect is inserted on the surface, the charge transference ΔQ and the potential V_{ES} influenced by the defect is then defined as

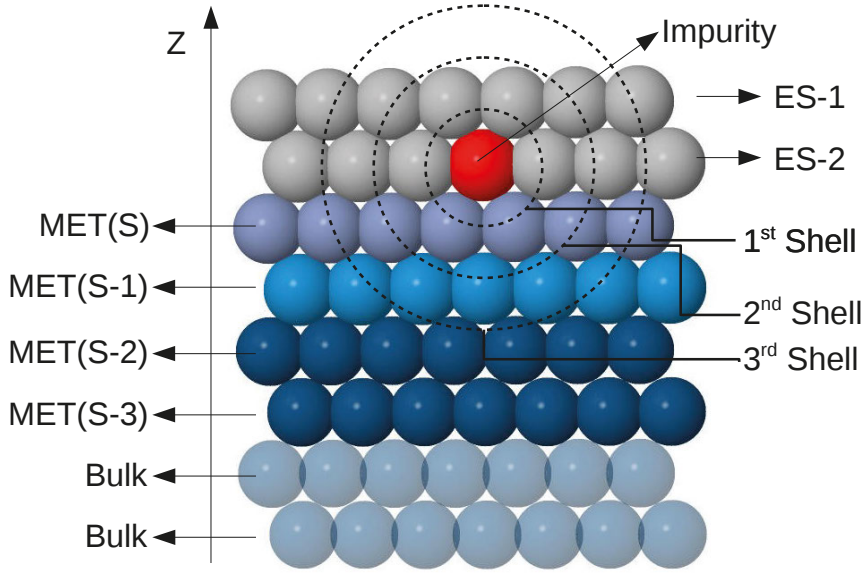

Figure 2.4. Schematic representation of the generic surface, including the defect denoted by the red color and its nearest neighbors denoted by the dashed concentric circles.

$$\Delta Q = \Delta Q_{surf} + \Delta Q_{local}, \tag{2.39}$$

$$V_E = V_{E_{surf}} + V_{E_{local}}, \tag{2.40}$$

where ΔQ_{surf} and $V_{E_{surf}}$ are the transferred charges and the electrostatic potential for the unperturbed surface, respectively, whereas ΔQ_{local} and $V_{E_{local}}$ are the transferred charges and the electrostatic potential associated with the perturbation, respectively.

Here, we give an example of one adsorbed atom on a metallic surface, called as impurity in the following. For that, the Fermi energy is fixed to the Fermi energy calculated for the corresponding bulk system without the defect. Then, the converged unperturbed surface is taken and we substitute one atom from the empty sphere layer ES-1 for one impurity. Now, in order to build the new Hamiltonian, an initial guess for the impurity potential parameters is taken, whereas for the other atoms of the other layers the potential parameters remain the same as those of the unperturbed surface. This procedure is the so called single site approach. Moreover, the recursion method is used to obtain the LDOS and $N_{RL}(E)$, integrating the latter until the Fermi energy according to Eqn. 2.38 in order to calculate the transferred charge ΔQ. In the next step,

the Eqn. 2.39 is used to calculate the charge transferred ΔQ_{local} on the impurity site. Using the charge conservation law, the charge in excess is distributed among the impurity neighbors and the electrostatic potential $V_{E_{local}}$ in the impurity site is determined by the resulting transferred charges. Once $V_{E_{local}}$ is found, $V_{E_{surf}}$ is added in order to obtain V_E according to Eqn. 2.40. Then, the new potential parameters are found in order to build the new Hamiltonian, repeating the process until the convergence is reached.

Once the single site calculation is converged, the nearest neighbors to the impurity are included in the self-consistent calculation. Then, all the process described previously is repeated until the convergence. More neighbors are included until we reach a point where there is no further influence on the impurity when including more neighborhood sites in the self-consistent calculation (see Fig. 2.4). This is the point where the calculation is considered to describe the problem at its highest efficiency.

It is important to notice that the geometry of the defect can be arbitrary since we are dealing with real space method. Therefore, the RS-LMTO-ASA is appropriate to treat nanostructures with no symmetry adsorbed or embedded in metallic surfaces. If one uses the reciprocal space approach, in order to calculate these nanostructures, a big supercell is needed to be used to prevent the nanostructure to interact with itself. Here, in the real space approach, one does not have to worry about such effect.

2.6.5 Non-collinear magnetism with RS-LMTO-ASA

In this section, a description of how the non-collinear magnetism is approached in the RS-LMTO-ASA method [56, 57] is provided. There are several methods in the literature that can deal with non-collinear magnetism of periodic system, but very few can deal with the non-collinear magnetism without any symmetry restrictions. Here, we will focus on the specific details to study the magnetization density in the RS-LMTO-ASA methods.

In the LSDA approximation, one can write the electronic density as a 2x2 density matrix, which would be a function of the non-magnetic charge n and the magnetization density $\mathbf{m}$, as following:

$$\rho = \frac{1}{2}(n\mathbf{1} + \mathbf{m}\cdot\sigma), \tag{2.41}$$

where $\mathbf{1}$ is the identity matrix 2x2 and $\sigma = (\sigma_x, \sigma_y, \sigma_z)$ are the Pauli matrices.

As shown in the recursion method (see Appendix B), the local density of states LDOS, $N(E)$, where E stands for the energy, is obtained by

$$N(E) = -\frac{1}{\pi}\Im Tr[G(E)], \tag{2.42}$$

where G is the Green function, which is described by

$$G(E) = (E - H)^{-1}, \tag{2.43}$$

with H being the Hamiltonian. The Green functions will be better explored in the next section.

Analogously to the LDOS calculation process, the collinear magnetization density can be calculated as

$$m(E) = -\frac{1}{\pi}\Im Tr[\sigma_z G(E)], \tag{2.44}$$

where only the diagonal elements of the Green function should be used. Therefore, in order to obtain a generalized non-collinear magnetization density, as the following is done:

$$\mathbf{m}(E) = -\frac{1}{\pi}\Im Tr[\sigma G(E)], \tag{2.45}$$

but for that it is necessary to calculate the non-diagonal terms of the Green function. Hence, it is clever to avoid to work with the non-diagonal terms, due its high computational costs.

With the RS-LMTO-ASA method, it is possible to avoid the calculation of these non-diagonal terms by doing unitary rotations U in the Hamiltonian. Therefore, if one performs rotations from σ to σ' in such a way that the component x of the matrix σ'_x gets to be diagonal, it is then possible to find $m_x(E)$. The same procedure can be done for the y component, obtaining then the full magnetization density vector $\mathbf{m}(E)$. When realizing unitary rotation on the Hamiltonian $H' = UHU^\dagger$, the Green function is rotated, therefore $G' = UGU^\dagger$. By knowing that the $U^\dagger U = 1$ and that the trace is invariant under rotations, one can write the generalized magnetization density of states as the following:

$$\mathbf{m}(E) = -\frac{1}{\pi}\Im Tr[\sigma U^\dagger U G U^\dagger U] = -\frac{1}{\pi}\Im Tr[\sigma' G'], \tag{2.46}$$

where σ' are the Pauli matrices after the unitary transformations.

Hence, one can choose two matrices, U_1 and U_2, in order to turn σ'_x and σ'_y diagonals and then calculate $m_x(E)$ and $m_y(E)$ through the diagonal elements of the Green function G. These rotations are in the spin space and described as

$$\sigma'_x = U_1 \sigma_x U_1^\dagger = \sigma_z, \tag{2.47}$$

and

$$\sigma'_y = U_2 \sigma_y U_2^\dagger = \sigma_y. \tag{2.48}$$

The Hamiltonian can be divided in a spin dependent part, called $\mathbf{B}$, and a spin independent part, called H^0, analogously to what was done in Eqn. 2.15. Therefore, one can write:

$$H' = H^0\mathbf{1} + \mathbf{B}\cdot U\sigma U^{\dagger}. \tag{2.49}$$

Now, the Hamiltonian matrix elements can be described using the LMTO parameters, in this case, in a first order representation. Here, the sites and orbitals will be denoted by $Q = RL$, the spin independent potential parameters will be denoted by the superscript 0 and the spin dependent potential parameters will be denoted by the superscript 1. Therefore, the spin independent and spin dependent part can be written, respectively, as

$$H^0_{QQ'} = \bar{C}^0_Q + \bar{\Delta}^{0\frac{1}{2}}_Q \bar{S}_{QQ'} \bar{\Delta}^{0\frac{1}{2}}_{Q'} + \bar{\Delta}^{1\frac{1}{2}}_Q \bar{S}_{QQ'} \bar{\Delta}^{1\frac{1}{2}}_{Q'} \mathbf{m}_Q \cdot \mathbf{m}_{Q'} \tag{2.50}$$

and

$$\mathbf{B}_{QQ'} = \left(\bar{C}^1_Q + \bar{\Delta}^{1\frac{1}{2}}_Q \bar{S}_{QQ'} \bar{\Delta}^{0\frac{1}{2}}_{Q'} \right) \mathbf{m}_Q + \bar{\Delta}^{0\frac{1}{2}}_Q \bar{S}_{QQ'} \bar{\Delta}^{1\frac{1}{2}}_{Q'} \mathbf{m}_{Q'} + \bar{\Delta}^{1\frac{1}{2}}_Q \bar{S}_{QQ'} \bar{\Delta}^{1\frac{1}{2}}_{Q'} \mathbf{m}_Q \times \mathbf{m}_{Q'}. \tag{2.51}$$

With the Hamiltonian described in Eqn. 2.49, the recursion method can be used three consecutive times for every one of the unitary transformations U_1, U_2 and U_3 in order to obtain $m_x(E)$, $m_y(E)$ and $m_z(E)$. With the magnetization density available, one can integrate the densities until the Fermi energy to obtain the magnetization of each direction and, therefore, to obtain the local spin moment direction.

2.6.6 The Bloch Spectral Functions in the real space

A significant part of the work developed in this thesis was the implementation of the Bloch Spectral Functions (BSF) calculation in the RS-LMTO-ASA method. Here follows an explanation on how these functions can be interpreted inside the real space and how it is interpreted by the code.

The local density of states (LDOS) can be written as a function of the intrasite Green function as the following:

$$N(E) = -\frac{1}{\pi}\Im G_0(E), \tag{2.52}$$

where the index 0 stands for a given site (for more details, see Appendix C). Therefore, one can define the BSF as the following manner:

$$A(\vec{k},E) = -\frac{1}{\pi}\Im G_0(\vec{k},E), \tag{2.53}$$

where $G_0(\vec{k},E)$ is the Fourier transformation of the real space Green function:

$$G_0(\vec{k},E) = \sum_j G_{0j}(E) \exp\left(\vec{k}\cdot\vec{R}_j\right). \tag{2.54}$$

If one integrates the BSF over the Brillouin Zone, the real space LDOS can be recovered as

$$N(E) = \frac{1}{\Omega_{BZ}} \int_{\Omega_{BZ}} A(\vec{k}, E) d^3\vec{k}. \tag{2.55}$$

One can verify it by using the Eqns. 2.53 and 2.54, writing the BSF as the following:

$$A(\vec{k}, E) = -\frac{1}{\pi} \Im \left[G_{00} + \sum_{j \neq 0} G_{0j} \exp\left(\vec{k} \cdot \vec{R}_j\right) \right]. \tag{2.56}$$

If one integrates both sides of Eqn. 2.56 over the Brillouin zone, it is possible to verify that only the first term, the intra-site term, is different than zero. This term is precisely the density of states in the real space, normalized by the Brillouin zone volume. Therefore, $A(\vec{k}, E)$ can be seen as the density of states project onto the reciprocal space. In the particular case of a perfectly ordered system $A(\vec{k}, E)$ is a sum of delta functions $\delta(E - E_{\vec{k}})$ that represent the dispersion relation $E_{\vec{k}}$.

The Green functions in the Eqns. 2.53 to 2.56 were calculated using the RS-LMTO-ASA. Since it is a code developed in the real space, one needs to check the convergence of the Eqn. 2.54. For that, one needs to compare the Green function between one atom on the site 0 and one atom in the first shell G_{01}, i.e. nearest neighbors, and the Green function between the atom on the site 0 and the last considered shell G_{0N}. If the Green function $G_{0N} \approx 0$ compared with the G_{01}, then one can conclude that contributions coming from further shells are negligible and the summation can be truncated. As the first test for this implementation, we have performed calculations for the bcc Fe bulk. In this way, it is possible to calculate the dispersion relation. This comparison is shown Fig. 2.5 and is possible to verify that the dispersion relation are in good concordance with the ones calculated in the reciprocal space. Although the real space bands are blurry due the imperfect description of the real space BSF, it is still possible to detect the most important features. The method used to make the comparison with is the Spin-Polarized Relativistic Korringa-Kohn-Rostoker electronic structure technique (SPR-KKR) [58]. The advantages of having such tool in the real space is the possibility to consider defect or impurities isolated and study how the bands respond to them. Another interesting application is the possibility to apply the developed implementation to finite objects.

In Paper **I**, we have applied it and calculated the energy dispersion for finite nanochains of Mn on Au(111) and Ag(111) surfaces. There, 17 Mn atoms were calculated self-consistently on top of the cited surfaces. After the self-consistent procedure, the Green functions and BSF were calculated, with the dispersion relation shown in Fig. 2.6. Note that the bands are very localized, i.e. it has a low dispersion due to the low dimension. The interesting

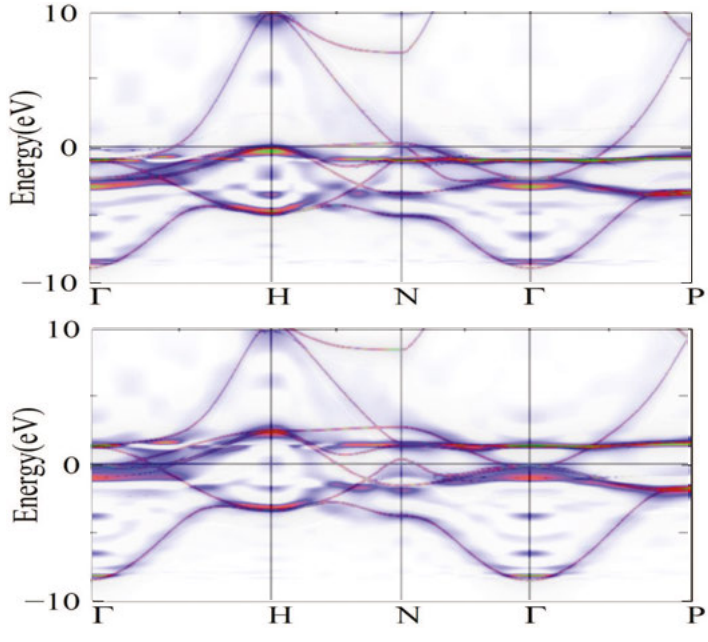

Figure 2.5. Bloch Spectral Function calculated for the Fe bcc bulk. In the upper part of the figure we have the majority bands, while in the bottom we have the minority bands. In the background of each figure is shown the dispersion relation calculated by the SPR-KKR method (black line) as comparison [58].

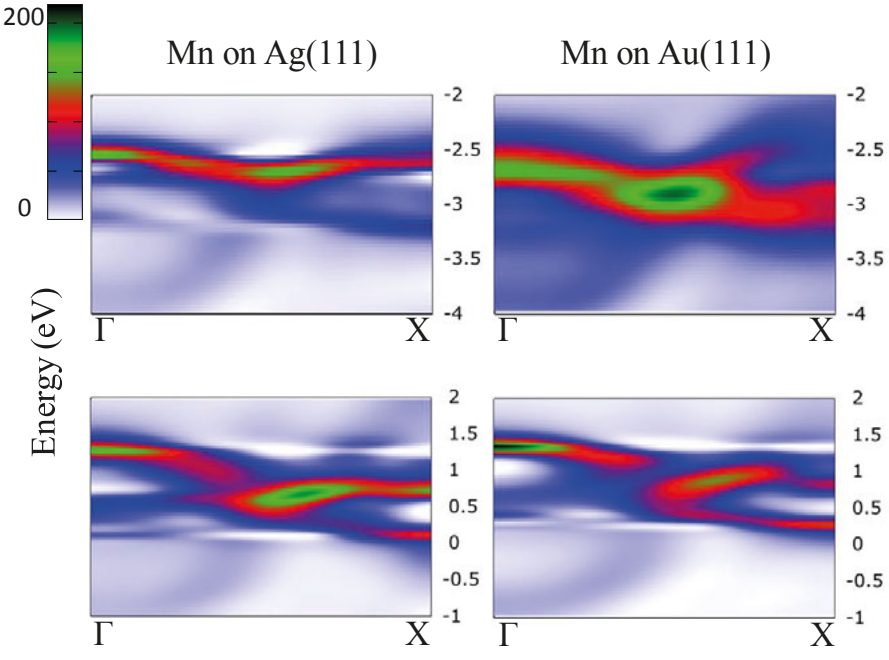

Figure 2.6. Bloch Spectral Function (BSF) calculated for the Mn nanochains on Ag(111) (left) and Au(111) (right) for the majority bands (top) and minority bands (bottom). The color gradient stands for the BSF values in arbitrary units.

fact here is that the dispersion relation, i.e. the energy and momentum transfer, is present even for finite materials, where the periodicity and boundary conditions are absent. For this case, an experimental verification of this, e.g. by use of angular resolved photo emission spectra (ARPES) would be highly interesting.

In order to test the convergence of the Eqn. 2.54, it was compared the Green function between the atom in the center of the nanochain (the atom that is supposed to have the parameters of a infinite nanochain) and its nearest neighbor with the Green function of the same central atom and the edge atoms, as shown in Fig. 2.7.

Note that the $G_{0-edge} \approx 0$ compared with G_{0-NN}. It shows that one can conclude that additional terms in the sum in Eqn. 2.54 will not influence the Fourier transformation and, consequently, the BSF calculation. More information can be found in the Paper **I**.

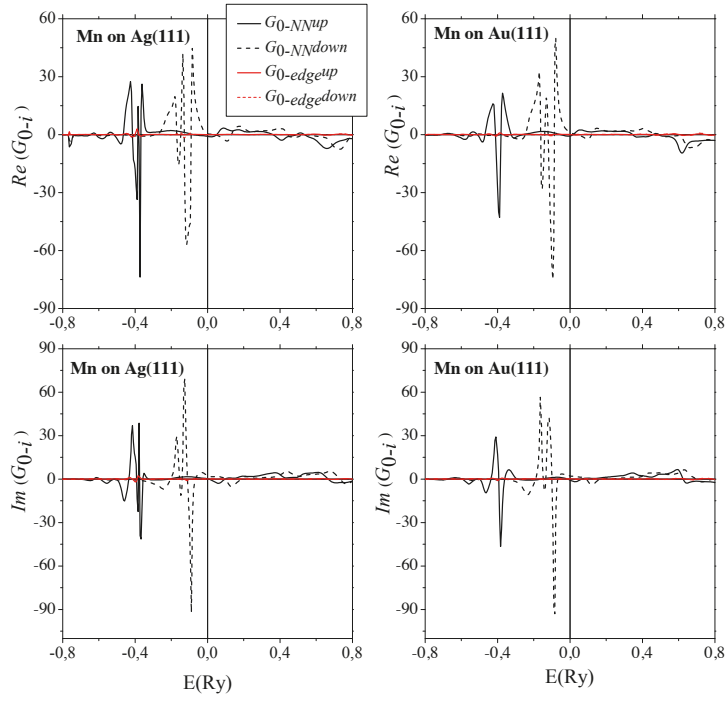

Figure 2.7. Comparison between the trace of the real part ($Re(G_{0-i})$) and imaginary part ($Im(G_{0-i})$) of the Green functions between the central atom and its nearest neighbor (G_{0-NN}) and between the central atom and the edge atom (G_{0-edge}).

3. Exchange parameters from the electronic structure: new insights and perspectives

In this chapter, we will show how the exchange coupling is calculated in the RS-LMTO-ASA method. Here, we extended the known formalism from collinear configuration [59–62] to a general non-collinear magnetic configuration [63]. Regarding the collinear formalism, we have deepened the interpretation and have projected the exchange coupling interaction J_{ij} into orbital resolved contributions, in case of cubic environment. The analysis has brought intriguing results which will be discussed in this chapter. Furthermore, we have used the non-collinear formalism to describe the Dzyaloshinskii-Moriya interaction (DMI). We have developed a computationally simple concept to directly calculate the x, y and z components, in cartesian coordinates, of the DMI vector in a global coordinate system for any non-collinear atomistic spin arrangement. Finally, we have extended the interpretation of each exchange parameter, J_{ij} and DMI, in order to understand both interactions in terms of spin and charge current.

3.1 The collinear exchange formula and the non-collinear exchange formalism

By means of Multiple Scattering Theory (MST) (see Appendix C), one can derive the two-site energy variation due to the Lloyd formula Eqn. 3.1 as follows

$$\delta E_{ij} = -\frac{1}{\pi}\Im \int_{-\infty}^{\varepsilon_F} d\varepsilon Tr_{\sigma L}\left(\delta \mathbf{P}_i \tau_{ij} \delta \mathbf{P}_j \tau_{ji}\right) . \tag{3.1}$$

This equation only describes the leading term of the energy variation when spins are rotated at site i and j at the same time (two-site rotation). This two-site energy variation can be derived for a spin Hamiltonian (like the Heisenberg model), and can be compared to Eqn. 3.1 by establishing a mapping procedure. Using the values for $\delta \mathbf{P}_i$ and τ_{ij}, defined in Eqns. C.34 and C.33, respectively, with $\delta \mathbf{P}_i$ being explicitly written as

$$\delta \mathbf{P}_i = p_i \delta \vec{e}_i \vec{\sigma}, \tag{3.2}$$

one can have

$$Tr_{\sigma L}(\delta P_i \tau_{ij} \delta P_j \tau_{ji}) = 2Tr_L\left(p_i T^0_{ij} p_j T^0_{ji} - p_i \vec{T}_{ij} p_j \vec{T}_{ji}\right)(\delta\vec{e}_i \delta\vec{e}_j) + 2Tr_L\left(p_i T^\alpha_{ij} p_j T^\beta_{ji} + p_j T^\beta_{ji} p_i T^\alpha_{ij}\right)\delta e^\alpha_i \delta e^\beta_j + 2Tr_L\left(p_i T^0_{ij} p_j \vec{T}_{ji} - p_j T^0_{ji} p_i \vec{T}_{ij}\right)(\delta\vec{e}_i \times \delta\vec{e}_j), \quad (3.3)$$

where indices α and β run over 0, x, y or z. A more detailed description about this derivation can be found in Ref. [63]. Using the properties of T_{ij} in the absence of spin-orbit coupling, one can have that

$$Tr_L\left(p_i T^\alpha_{ij} p_j T^\beta_{ji}\right) = Tr_L\left(p_j T^\beta_{ji} p_i T^\alpha_{ij}\right), \quad (3.4)$$

thus, the third term of Eqn. 3.3 is null. Introducing the matrices

$$A^{\alpha\beta}_{ij} = \frac{1}{\pi}\Im \int_{-\infty}^{\varepsilon_F} d\varepsilon Tr_L\left(p_i T^\alpha_{ij} p_j T^\beta_{ji}\right) \quad (3.5)$$

and the matrix

$$\hat{A}^{\alpha\beta}_{ij} = \frac{1}{\pi}\Re \int_{-\infty}^{\varepsilon_F} d\varepsilon Tr_L\left(p_i T^\alpha_{ij} p_j T^\beta_{ji}\right), \quad (3.6)$$

one can write the energy variation as

$$\delta E_{ij} = -2\left(A^{00}_{ij} - \sum_{\mu=x,y,z} A^{\mu\mu}_{ij}\right)\delta\vec{e}_i \delta\vec{e}_j - 4\sum_{\mu,\nu=x,y,z} \delta e^\mu_i A^{\mu\nu}_{ij} \delta e^\nu_j . \quad (3.7)$$

In Eqn. 3.7 one can identify the first term as the LKAG exchange coupling (in case of collinear spin configurations) and the second term as an anisotropy term that may be non-zero even in the absence of the spin-orbit coupling, as explored in more detail in Paper **V**. Now, one can add the spin-orbit coupling as a perturbation and for that we make a few remarks about how to treat perturbations in the MST.

Let us add the spin-orbit coupling as a perturbation. Then one has to calculate the perturbed $\delta\mathbf{P}'$-s and τ'-s. It can be shown that the perturbed Green-function can be given as

$$\mathbf{G}'_{ij} = \mathbf{G}^0_{ij} + \Delta\mathbf{G}_{ij}, \quad (3.8)$$

where $\mathbf{G}^0_{ij}$ has the structure of $G^0_{ij} I_2$, while $\Delta\mathbf{G}_{ij}$ can be formed as $\xi\vec{\Gamma}_{ij}\vec{\sigma}$, with ξ being the strength of the spin-orbit coupling and the component Γ^μ_{ij} is obtained as

$$\Gamma_{ij}^{\mu} = \sum_{k} \mathbf{G}_{ik}^{0} L^{\mu} \mathbf{G}_{kj}^{0} \tag{3.9}$$

where L^{μ} is a component of the angular momentum operator. This implies that $\vec{\Gamma}_{ij}$ transforms as

$$\left(\Gamma_{ij}^{\mu}\right)^{T} = -\Gamma_{ji}^{\mu} , \tag{3.10}$$

where μ runs over the coordinates x, y and z. For further details of the derivation of the vector $\vec{\Gamma}_{ij}$, see the BSc Thesis of A. Deák, Ref. [64]. Using $\Delta\mathbf{G}_{ij} = \xi\vec{\Gamma}_{ij}\vec{\sigma}$, one gets that

$$\left(\mathbf{t}_{i}'\right)^{-1} = \mathbf{t}_{i}^{-1} - \xi\left(\vec{\Gamma}_{ii}\vec{\sigma}\right) , \tag{3.11}$$

i.e.

$$\mathbf{P}_{i}' \simeq \mathbf{P}_{i} - \xi\left(\vec{\Gamma}_{ii}\vec{\sigma}\right) = p_{i}^{0} + \left(p_{i}\vec{n}_{i} - \xi\vec{\Gamma}_{ii}\right)\vec{\sigma} . \tag{3.12}$$

It implies that

$$\delta\mathbf{P}_{i}' \simeq p_{i}\delta\vec{n}_{i}\vec{\sigma} = \delta\mathbf{P}_{i} . \tag{3.13}$$

Now, the final task is to calculate the τ'. Considering Eqns. C.33 and C.34, one can write for the perturbed scattering path operator that

$$\tau_{nm}' = \mathbf{t}_{n}\delta_{nm} + \sum_{k\neq n} \mathbf{t}_{n}\mathbf{G}_{nk}'\tau_{km} , \tag{3.14}$$

with $\mathbf{G}_{nk}'$ being the perturbed Green function considering the spin-orbit coupling. That should be applied to $\mathbf{t}_{i}'$, see Eqn. 3.8. It is possible to get that, changing the indices n, m to i, j

$$\tau_{ij}' = \tau_{ij} + \Delta\tau_{ij} , \tag{3.15}$$

where

$$\Delta\tau_{ij} = \xi\mathbf{t}_{i}\left(\vec{\Gamma}_{ii}\vec{\sigma}\right)\mathbf{t}_{i}\delta_{ij} + \xi\mathbf{t}_{i}\left(\vec{\Gamma}_{ii}\vec{\sigma}\right)\mathbf{t}_{i}\mathbf{G}_{ij}^{0}\mathbf{t}_{j} + \xi\mathbf{t}_{i}\mathbf{G}_{ij}^{0}\mathbf{t}_{j}\left(\vec{\Gamma}_{jj}\vec{\sigma}\right)\mathbf{t}_{j} + \xi\mathbf{t}_{i}\left(\vec{\Gamma}_{ij}\vec{\sigma}\right)\mathbf{t}_{j} . \tag{3.16}$$

Note that site i is never equal site j in this formula. One can prove that $\Delta\tau_{ij}$ has the same structure as τ_{ij}, i.e.

$$\Delta\tau_{ij} = \Delta T_{ij}^{0} I_{2} + \Delta\vec{T}_{ij}\vec{\sigma} . \tag{3.17}$$

Using Eqns. 3.10 and 3.16, it can be shown that

$$\left(\Delta T_{ij}^{\alpha}\right)^{T} = -\Delta T_{ji}^{\alpha} . \tag{3.18}$$

This implies that

$$Tr_L\left(p_i\Delta T_{ij}^{\alpha}p_jT_{ji}^{\beta}\right)=-Tr_L\left(p_iT_{ij}^{\beta}p_j\Delta T_{ji}^{\alpha}\right) \tag{3.19}$$

and

$$Tr_L\left(p_iT_{ij}^{\alpha}p_j\Delta T_{ji}^{\beta}\right)=-Tr_L\left(p_i\Delta T_{ij}^{\beta}p_jT_{ji}^{\alpha}\right)\ . \tag{3.20}$$

With the properties described by Eqns. 3.19 and 3.20, the third term of Eqn. 3.7 is no longer null, therefore, the energy variation now has the form of

$$\delta E_{ij}=-2\left(A_{ij}^{00}-\sum_{\mu=x,y,z}A_{ij}^{\mu\mu}\right)\delta\vec{e}_i\delta\vec{e}_j-4\sum_{\mu,\nu=x,y,z}\delta e_i^{\mu}A_{ij}^{\mu\nu}\delta e_j^{\nu}-2\vec{D}_{ij}\left(\delta\vec{e}_i\times\delta\vec{e}_j\right)\ . \tag{3.21}$$

Lastly, after the mapping into the Heisenberg Hamiltonian, one can extract the value for both exchange coupling J_{ij}, the Dzyaloshinskii-Moriya vector $\vec{D}_{ij}$ (which will be further discussed in the next section) and an anisotropy term already mentioned. The quantities J_{ij} and $\vec{D}_{ij}$, in terms of Eqns. 3.5 and 3.6, can be written as

$$J_{ij}=A_{ij}^{00}-A_{ij}^{xx}-A_{ij}^{yy}-A_{ij}^{zz}, \tag{3.22}$$

and

$$\vec{D}_{ij}=\hat{A}_{ij}^{0\mu}-\hat{A}_{ij}^{\mu 0}\,. \tag{3.23}$$

The LKAG mapping is correct because the anisotropy term does give a contribution that is being of fourth order in the angle variation taken by rotating the two interacting spins, see Ref. [65]. It can however be shown that the second term in Eqn. 3.21 does not give significant contribution when a flat spin spiral is considered. This is an other case of the exact mapping, beside the collinear LKAG limit, that can be the subject for further studies. Note that in a non-equlibrium - non-collinear case, the anisotropy term gives non-trivial contributions, even in the case of bulk bcc Fe, as it has been shown in Ref. [66].

3.2 Exchange formulas in RS-LMTO-ASA

The connection between the parameters in terms of the MST and the LMTO is not so simple. In a general way, we have that $p=\frac{C-E_v}{\Delta}$ and $T=\sqrt{\Delta}G\sqrt{\Delta}$ [67]. With these substitution, entities with the form of $p_iT_{ij}p_jT_{ji}$ assumes the form of $\frac{1}{4}\delta_iG_{ij}\delta_jG_{ji}$, where δ is the energy-dependent local exchange splitting matrix. In this way, the new equation for the A_{ij} matrices can be written as

$$A_{ij}^{\alpha\beta,KKR} \equiv \frac{1}{\pi}\int_{-\infty}^{\varepsilon_F} d\varepsilon \,\mathrm{Im}\, Tr_L\left(p_i T_{ij}^{\alpha} p_j T_{ji}^{\beta}\right) = \frac{1}{4\pi}\int_{-\infty}^{\varepsilon_F} d\varepsilon \,\mathrm{Im}\, Tr_L\left(\delta_i G_{ij}^{\alpha} \delta_j G_{ji}^{\beta}\right), \tag{3.24}$$

and δ_i has the form of

$$\delta_i(\varepsilon) \equiv \frac{C_i^{\downarrow}\Delta_i^{\uparrow} - C_i^{\uparrow}\Delta_i^{\downarrow} + \left(\Delta_i^{\downarrow} - \Delta_i^{\uparrow}\right)\varepsilon}{\sqrt{\Delta_i^{\downarrow}\Delta_i^{\uparrow}}}\,. \tag{3.25}$$

A more detailed description of such correspondence can be seen in Ref. [63]. Moreover, a slightly more complicated correspondence comes from intra-site terms such $p_i T_{ii}$. In this case, the description can be found in Ref. [60].

3.3 Dzyaloshinskii-Moriya interaction

Recently, a lot have been discussed about the new limits of the current technology, as the devices get smaller and smaller. Particularly, concerning data storage, new solutions are being researched as we reach the size limits for thin films. A good alternative has been shown with the topologically protected magnetic configuration, so called skyrmions [34–42]. In this size limit, some interactions get to be more and more important. One of those key interactions is the Dzyaloshinskii-Moriya interaction, which is crucial for the stabilization of the skyrmionic phase. In this section, we will show a few preliminary tests and further results obtained after the implementation of the DMI calculation in the RS-LMTO-ASA method.

After the whole self-consistent procedure, i.e. after having all the converged potential parameters, it is possible to compute the Green functions for the studied system. In the following tables, we will show how the matrices of Eqn. 3.23 change from regime to regime, showing the finite $\vec{D}_{ij}$ when the symmetry is broken. Note that the structure of the matrices are the same for both A_{ij} and $\hat{A}_{ij}$

Table 3.1. *The structure of $A_{ij}^{\alpha\beta}$ in the lack of spin-orbit coupling, considering a collinear magnetic configuration, for bulk system. This is the case for both A_{ij} and $\hat{A}_{ij}$.*

$A_{ij}^{\alpha\beta}$	0	x	y	z
0	a	0	0	c
x	0	0	0	0
y	0	0	0	0
z	c	0	0	b

Table 3.2. *The structure of $A_{ij}^{\alpha\beta}$ in the presence of spin-orbit coupling, considering a collinear magnetic configuration, for bulk system. This is the case for both A_{ij} and $\hat{A}_{ij}$.*

$A_{ij}^{\alpha\beta}$	0	x	y	z
0	a	d	e	c
x	d	i	f	g
y	e	f	j	h
z	c	g	h	b

Table 3.3. *The structure of $A_{ij}^{\alpha\beta}$ in the presence of spin-orbit coupling, considering a collinear magnetic configuration, for surface system. This is the case for both A_{ij} and $\hat{A}_{ij}$.*

$A_{ij}^{\alpha\beta}$	0	x	y	z
0	a	d'	e'	c'
x	d	i	f'	g'
y	e	f	j	h'
z	c	g	h	b

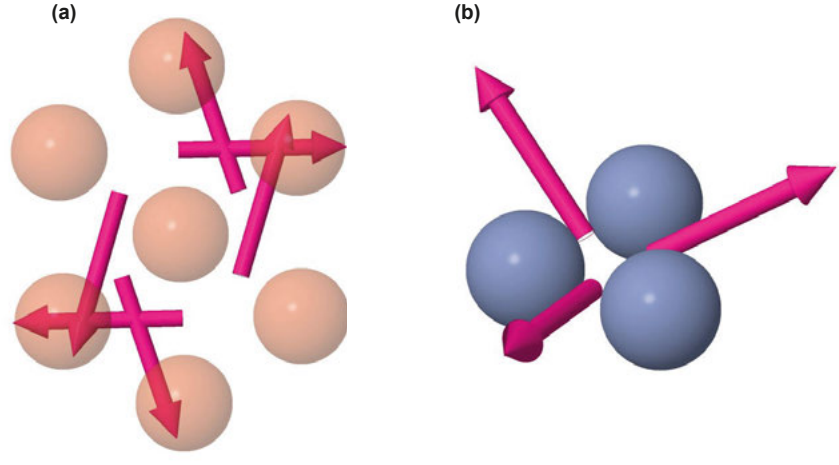

Figure 3.1. Schematic representation of the (a) Fe monolayer on W(110) and the (b) triangular trimer of Cr on Au(111), where in the former one is only represented the central atom and its nearest and next nearest neighbors. The pink arrows denote the normalized DMI direction and they stand in between two atoms which the interaction correspond to.

Considering the spin-orbit coupling and the broken symmetry, one can verify that in Table 3.3, the $\hat{A}_{ij}^{\alpha\beta}$ matrix is no longer symmetric, which means that the $\vec{D}_{ij}$ is now different than zero. In order to test our new implementation, we have applied the formalism to calculate the DMI for systems where results have been shown in the literature. Particularly, for a monolayer of Fe on W(110) and a triangular trimer of Cr on Au(111), with results shown in the Refs. [68] and [69], respectively. One can verify that the results of the DMI are in a good agreement with the cited literature. This good agreement encourages us then to study new results for new systems.

It is noteworthy to say that since RS-LMTO-ASA is a real space method, it gives us the freedom to calculate all the components of the DMI vector for any nanostructure with any magnetic structure. In paper **VI** we explored this potential by calculating the DMI for triangular trimers on top of Au(111) and Ag(111), revealing its direction, strength and how does it behave between different substrate and magnetic configuration.

3.4 Orbital resolved J_{ij}

The Beth-Slater (BS) curve is part of a fundamental understanding of the magnetism and the magnetic ordering of the 3d transition metals. It can explain the anti-ferromagnetic (AFM) behavior of bcc Cr, as well as the ferromagnetism of bcc Fe, hcp Co and fcc Ni, for example. Here, the mechanism behind the curve will be revisited with a deeper analysis.

This analysis consists in considering the cubic symmetry of the 3d transition metals and examining the individual influence of its orbitals. In the case of cubic symmetry, the d orbitals (which provides the biggest contribution to the J_{ij}) split in two different irreducible representations inside the point symmetry, the E_g and T_{2g}. In Eqn. 3.22, the multiplication of the Green functions matrices will give rise to elements that will have purely T_{2g} or E_g contributions, but as well as mix terms such as $T_{2g} - E_g$. In this way, one can rewrite the total J_{ij} as

$$J_{ij} = J_{ij}^{E_g - E_g} + J_{ij}^{E_g - T_{2g}} + J_{ij}^{T_{2g} - T_{2g}}, \tag{3.26}$$

where $J_{ij}^{E_g - E_g}$ is the contribution coming from the interaction exclusively between orbitals E_g, $J_{ij}^{T_{2g} - T_{2g}}$ from T_{2g} orbitals and the term coming from the interaction between both orbitals, $J_{ij}^{E_g - T_{2g}}$. The J_{ij} between the nearest neighbors (NN) and next-nearest neighbors (NNN) were calculated for the 3d metals in bcc structure and shown in Fig. 3.2

Note that the contribution coming $T_{2g} - T_{2g}$ between NN for bcc Fe is a relatively strong AFM contribution compared with the total ferromagnetic (FM) contribution already known from the literature**??**. Depending on how Fe is

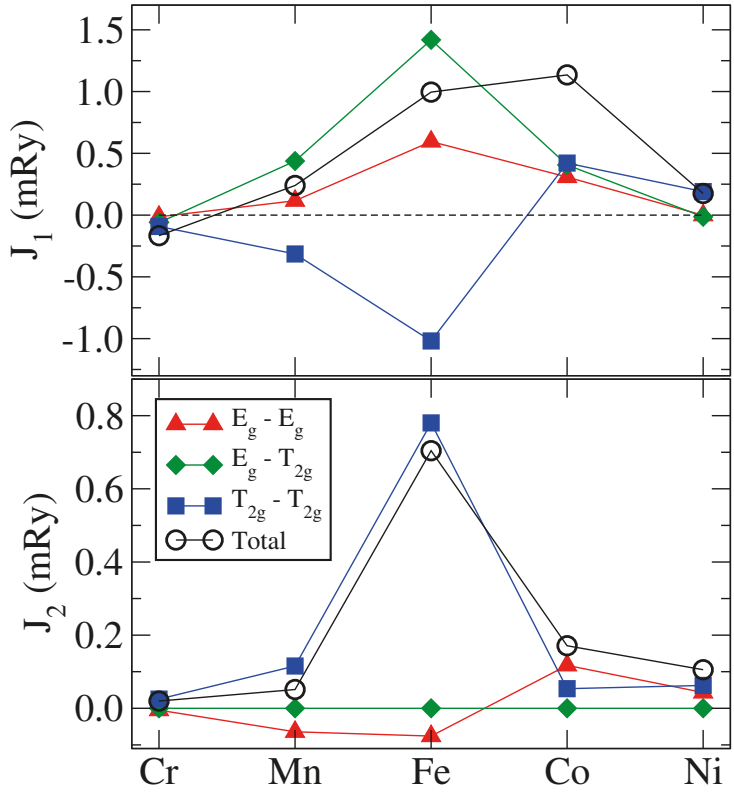

Figure 3.2. Exchange coupling J_{ij} between the NN (J_1) and NNN (J_2) project onto orbitals T_{2g} and E_g for $3d$ metals in bcc structure.

inserted in the system, such as an alloy, the interaction between nearest neighbors can bring significant AFM contribution. More about this subject is further explored in Papers **II**, **III**, **IV** and **V**.

3.5 Influence of spin and charge current in the exchange interactions

Still looking to improve the understanding of the exchange interactions, a good idea that could enlighten the understanding of them and create a insightful connection with the experiments is to study them as a function of spin and charge currents. Here, the Green functions can be divided into both spin independent $\left(G^0_{ij}\right)$ and spin dependent $\left(G^{\mu}_{ij}\right)$, being 9×9 matrices with orbital indexes written here as α, β. Then, one can represent these Green function in terms of their behavior under a given operation T, an operator that simultaneously transpose orbitals and sites. Firstly, one can rewrite the Green functions as

$$G^0_{ij} = G^{00}_{ij} + G^{01}_{ij} \tag{3.27}$$

and

$$G^{\mu}_{ij} = G^{\mu 0}_{ij} + G^{\mu 1}_{ij}\,, \tag{3.28}$$

where the second index, that was introduced in Eqns. 3.27 and 3.28, denotes whether it is even (0) or odd (1) under T, meaning that

$$\left(G^{00}_{ij\alpha\beta}\right)^T = G^{00}_{ji\beta\alpha} = G^{00}_{ij\alpha\beta}, \tag{3.29}$$

$$\left(G^{01}_{ij\alpha\beta}\right)^T = G^{01}_{ji\beta\alpha} = -G^{01}_{ij\alpha\beta}. \tag{3.30}$$

Lastly, the two-index formalism can be obtained with the one-index formalism from

$$G^0_{ij} + {G^0_{ij}}^T = G^{00}_{ij} + G^{01}_{ij} + \left(G^{00}_{ij} + G^{01}_{ij}\right)^T = G^{00}_{ij} + G^{01}_{ij} + G^{00}_{ij} - G^{01}_{ij} = 2G^{00}_{ij} \tag{3.31}$$

$$G^0_{ij} - {G^0_{ij}}^T = G^{00}_{ij} + G^{01}_{ij} - \left(G^{00}_{ij} + G^{01}_{ij}\right)^T = G^{00}_{ij} + G^{01}_{ij} - G^{00}_{ij} + G^{01}_{ij} = 2G^{01}_{ij}\,. \tag{3.32}$$

The four different parts of the decomposed Green function have direct physical origins as tabulated below

G^{00}	charge density
G^{01}	charge current
$G^{\mu 0}$	spin density
$G^{\mu 1}$	spin current

Then, it is straightforward to rewrite Eqn. 3.23 as

$$D^{\mu}_{ij} = \frac{1}{2\pi}\Re\int \mathrm{Tr}\left\{\delta_i G^{00}_{ij}\delta_j G^{\mu 1}_{ji} + \delta_i G^{01}_{ij}\delta_j G^{\mu 0}_{ji}\right\} = \left(D^S_{ij} + D^C_{ij}\right)^{\mu}. \tag{3.33}$$

With this formulation, we have divided the DMI in two parts. One related with the spin-current, called $D^S \propto G^{00}G^{\mu 1}$; and other one related with the charge-current $D^C \propto G^{01}G^{\mu 0}$. In this interpretation of DMI, it arises due to inter-atomic spin and charge currents.

We also implemented the same line of thought to calculate the exchange parameter J_{ij}, rewriting Eqn. 3.22 as

$$J_{ij} = \frac{1}{8\pi}\Im\int \mathrm{Tr}\left\{\delta_i G^{00}_{ij}\delta_j G^{00}_{ji} + \delta_i G^{01}_{ij}\delta_j G^{01}_{ji} - \delta_i G^{0\mu}_{ij}\delta_j G^{0\mu}_{ji} - \delta_i G^{1\mu}_{ij}\delta_j G^{1\mu}_{ji}\right\}. \tag{3.34}$$

Note that when the superscript μ is repeated, a summation is implicit. In this way, one can interpret the total J_{ij} as a sum of four different parts. One related

with the charge density J_{ij}^{CD}, one with the charge current J_{ij}^{CC}, one with the spin density J_{ij}^{SD} and one with the spin-current J_{ij}^{SC},

$$J_{ij} = J_{ij}^{CD} + J_{ij}^{CC} - J_{ij}^{SD} - J_{ij}^{SC}. \tag{3.35}$$

Note that here we suppress the integration variable as well as its limits, in order to simplify the equation. Recently the existence of orbital magnetic moment in absence of SOC that is driven by the spin chirality of a given system have been discussed e.g. in [70, 71]. Here, we have performed calculations including SOC and once converged one can scale its strength down to zero. We used this scaling to study the influence of the SOC on DMI vectors calculated for systems where the magnetic configuration gives rise to a spin chirality different than 0. For simplicity, here we only present calculations for a Mn triangular trimer on Ir(111) and Au(111) surfaces, and analysed three different scenarios: (1) a rotation from a ferromagnetic configuration to a Neél structure and further back to a ferromagnetic configuration after a 180° rotation. Note that in between the collinear configurations, the in-plane angle of 120° was fixed between the magnetic moments; (2) a scaling of the strength of SOC, when the magnetic moments have an in-plane angle of 120° between them and with a 40° with respect to the z-axis; and (3) a global spin rotation, R_α, of the magnetic configuration described in (2), around the y-axis with an angle α. Once the rotation is done, we calculate the new DMI and rotate back to the original reference frame.

In Fig. 3.3 we show results from calculation for the Mn trimer on Au(111) and Ir(111) at every 10°, from 0° to 180°. A self-consistent calculation was made for every 10° step. Our results show that when the magnetic configuration is collinear, the DMI only exists if the SOC is different from zero, meaning that there is no non-relativistic contribution to it. However, when a non-coplanar magnetic configuration ($\vec{S}_i \times \vec{S}_j \cdot \vec{S}_k \neq 0$) is reached, the non-relativistic part of the DMI dominates and in fact there is a very small difference between values with and without SOC. It is noteworthy to say that when $\theta = 90°$, i.e. a Néel magnetic structure, the spin chirality is zero and there is no charge-current flowing in the system. This means that the charge-current dependent part of the DMI D^C vanishes and all the contribution comes from the spin-current dependent D^S, whose z-component is allowed by symmetry. The relation between DMI and spin current have been recently argued [71,74].

In Fig. 3.4 we converged the system with the magnetic moments at an angle $\theta = 40°$ with respect to the z-axis. Then we scaled the strength of SOC to study its influence on the DMI. One can verify in Fig. 3.4 that there is a very weak influence, corroborating our statement that, for this system and this configuration, the source of the DMI is primarily due the non-relativistic sources.

In Fig. 3.5 we repeated the set up of Fig. 3.4 but did a global spin rotation, R_α, of the magnetic configuration around the y-axis. The non-relativistic part

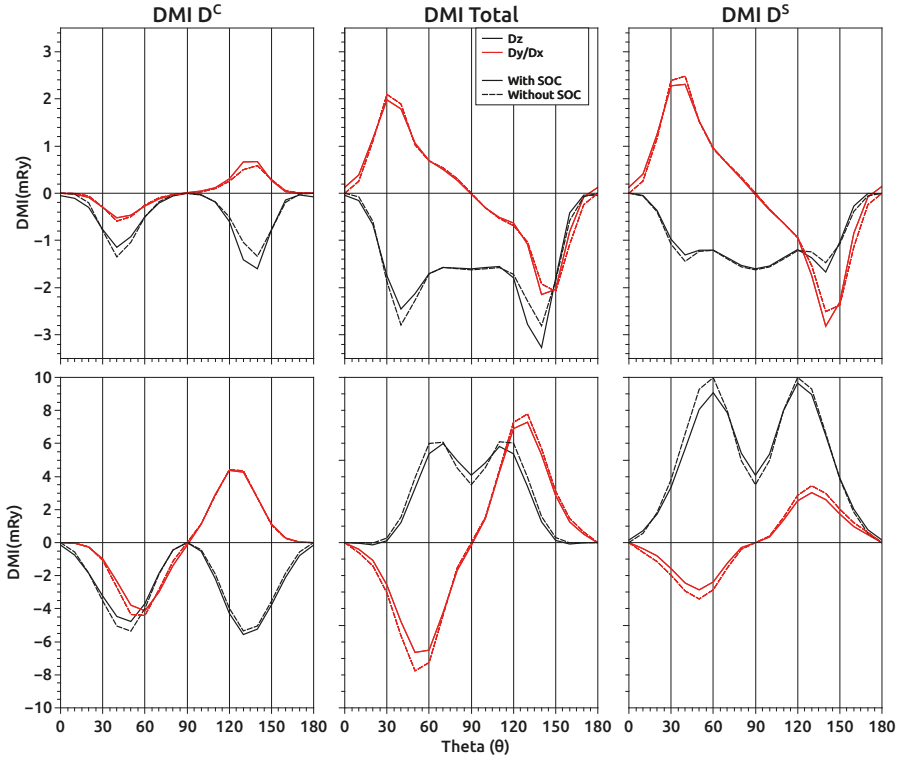

Figure 3.3. DMI calculated when varying the vertical angle of the magnetic moments between $\theta = 0^\circ$ and $\theta = 180^\circ$. On top we have the plot for Mn triangular trimer on Ir(111) and on bottom the Mn triangular trimer on Au(111). The black line denotes the D_z component while the red line denotes the in-plane component D_y/D_x. The full line stands for the calculation when the spin-orbit coupling is included, whereas the dashed line denotes the calculation without spin-orbit coupling.

of DMI should be scalar in spin space, therefore for zero SOC $\vec{D}_{ij}(\alpha)\cdot R_\alpha \hat{e}_i \times R_\alpha \hat{e}_j = \vec{D}_{ij}(0)\cdot \hat{e}_i \times \hat{e}_j$. In the limit of weak SOC the quantity $R_\alpha^{-1}\vec{D}_{ij}(\alpha) \approx \vec{D}_{ij}(0)$ should be fairly independent of α with any anisotropy directly connected to the SOC. The result is shown in Fig. 3.5. One can verify an almost constant value for the DMI with very small oscillations. We can conclude that again, for that configuration, the DMI is present mostly due to non-relativistic effects, although the small oscillations refers to some small relativistic effects, probably related with one-site anisotropy.

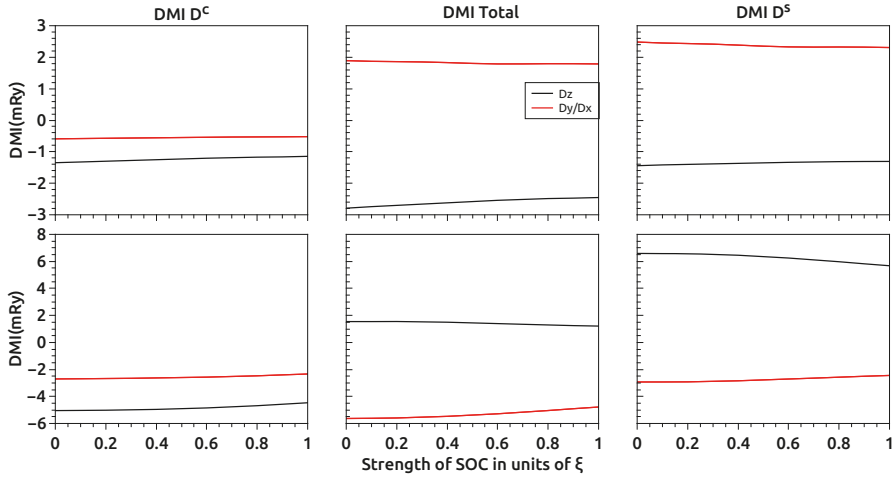

Figure 3.4. Scaling of the strength of the SOC calculated for a Neél like magnetic structure with a fixed θ =40°. On top we have the plot for Mn triangular trimer on Ir(111) and on bottom the Mn triangular trimer on Au(111). The black line denotes the D_z component while the red line denotes the in-plane component D_y/D_x.

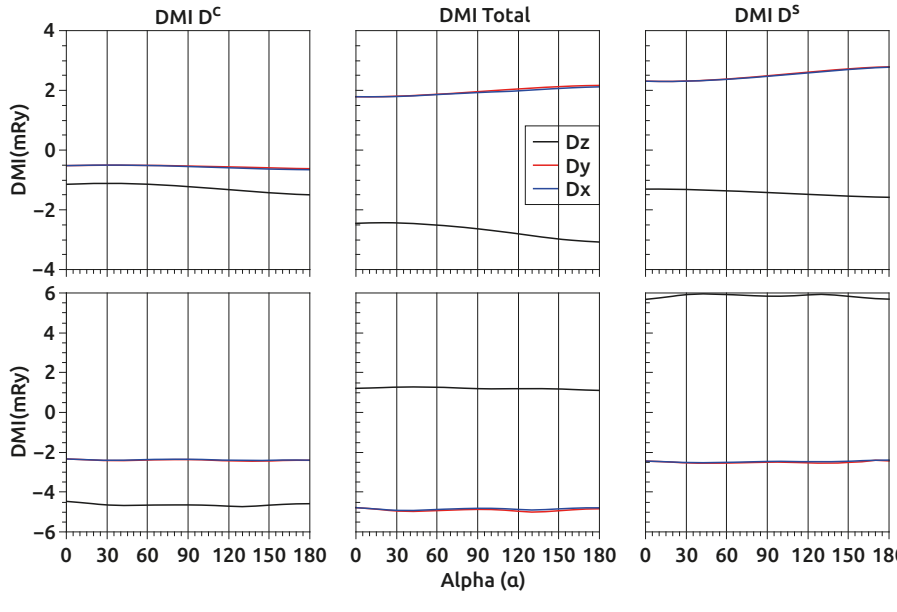

Figure 3.5. Calculated DMI when one perform a global spin rotation of the magnetic structure by angle α around the y-axis. On top we have the plot for Mn triangular trimer on Ir(111) and on bottom the Mn triangular trimer on Au(111).

4. Introduction to the papers

This chapter will be dedicated to detail the importance of study presented in this thesis for each paper. The content for each paper is discussed around a new interpretation of the well known exchange-coupling parameter J_{ij} and the Dzyaloshinskii-Moriya interaction D_{ij} for several different systems. The contribution done by me for the papers are the following

- In Paper **I**, I performed most of the calculations concerning to the electronic structure of the 1D Mn systems on Ag(111) and Au(111), as well as calculated the J_{ij} and its new features implemented by me. Among the new features, that were implemented and presented in the paper, the calculation of the J_{ij} as a function of energy was particularly important to show how sensitive the 1D systems are to effects such as hybridisation and coordination number, consequently. Lastly, I also implemented how to calculated the Bloch Spectral Function (BSF).
- In Paper **II**, **III** and **V**, another implementation done in the RS-LMTO-ASA was used, in which the J_{ij} was split into orbital contributions to study how each orbital contributes to the total J_{ij}. In addition to the implementation and calculations, I have participated actively in the discussions presented in the papers.
- In Paper **IV**, I have calculated the electronic structure using the RS-LMTO-ASA method for the bulk materials and participated actively on the analysis of the data.
- In Paper **VI**, I have calculated the electronic structure for the triangular trimers on top of Ag(111) and Au(111) surfaces. There, it was also implemented the calculation of the D_{ij} and revealed its strength and direction for these nanostructures, considering different magnetic configurations.

4.1 Magnetic and electronic structure of 1d Mn nanostructures on Ag(111) and Au(111)

In Paper **I**, *ab initio* calculation of 1D Mn nanostructures on Ag(111) and Au(111) was shown. For Mn chains on Ag(111), our calculations have shown that the edge atoms in general have canted orientation compared to the Mn atoms in the center of the chain, which present collinear configuration. This is supported by the fact that the J_{ij} is slightly different in the edge, given by a competition between nearest (NN) and next-nearest neighbor (NNN), leading

to the canted orientation. In the middle of the chain, this competition is weaker and the collinear ferromagnetic configuration prevails. For the Mn chains on Au(111) the magnetic behavior is different, where in general the orientations between all Mn atoms are noncollinear. Furthermore, since we find that Mn atoms on Ag and Au surfaces in general present exchange coupling parameters with the same magnitude and sign, it is reasonable to conclude that stronger spin-orbit coupling of the Au substrate, leads to non negligible effects from the Dzyaloshinskii-Moriya interaction, which is known to favor noncollinear magnetism. Lastly, a method to obtain energy bands from real-space Green functions was developed, by considering a Fourier transform. We have shown that energy bands can be observed even for finite-size objects like the systems considered here. As mentioned before, an experimental verification of such theoretical finding using, for example, angular resolved photo emission spectra (ARPES) would be of great interest.

4.2 Orbital resolved J_{ij} for Cr, Mn, Fe, Co and Ni

The implementation of the calculation of orbital resolved J_{ij} is presented in several papers presented in this thesis. In Paper **II**, we have shown that the well known Bethe-Slater curve does not follow the same pattern observed for the total J_{ij}. This gives us new insights about the electronic structure and the magnetism of each metal. Firstly, for the NN exchange-coupling interaction $J'_{ij}s$, for the bcc lattice metals, we find that the $E_g - E_g$ contributions are ferromagnetic throughout the 3d series, once the E_g orbitals are populated. The T_{2g} orbitals are populated very close to the Fermi surface, meaning that they are very sensitive to the chemical potential, leading to the coupling between them to be ferromagnetic or anti-ferromagnetic. In this scenario, the coupling between T_{2g} and E_g shows itself not straightforward and depending heavily on each orbital filling. These findings about each orbital have revealed that, for a particular direction ([111] in this case), the long-range interaction is mostly done by the T_{2g} electrons due to the fact that the Fermi surface is formed almost exclusively by T_{2g} electrons. Lastly, we have shown that for the $T_{2g} - E_g$ coupling, due to the complexity present in the interplay between both orbitals, the trend is not so trivial. An interesting fact is that, due to symmetry reasons, the mixed coupling is null between NNN, i.e. between atoms in the borders of the cube. This is simply due the fact that, in this case where atoms obey the C_{4v} symmetry, there is not a matrix that can transform one E_g orbital into T_{2g} orbital, therefore, they do not mix with each other. All these information combined can enlighten the discussion of new magnetic materials design, opening new windows and perspectives for the experimentalists who work in this field.

From the discussion above, one metal showed particularly an intriguing result. This leads us to Paper **III**, where we discuss the particular case for the bcc Fe. In this paper, we discuss form a microscopic level showing the dif-

ference between E_g and T_{2g} orbitals, revealing their particular contribution to the microscopic known behavior of bcc Fe. The T_{2g} orbital, as already mentioned for other metals above, shapes the Fermi surface, while the E_g forms weakly interacting impurity levels. Due to these particular characteristics, the T_{2g} orbital does not show a big dependence on the magnetic configuration and is classified to be Heisenberg-like, whereas the E_g orbital break this scenario, since it highly depends on the spin orientation. In the end, the analysis of the nearest neighbor exchange-coupling interaction between T_{2g} orbitals are negative (antiferromagnetic), despite the total J_{ij} being strongly ferromagnetic, due these couplings being driven by Fermi surface nesting. We argue then that bcc Fe has a unique behavior among other $3d$ metals when it comes to magnetic exchange interactions.

Still about Fe and its unique behavior, we reach Paper **V**. It takes the analysis in Paper **III** to a different level: mapping into a bilinear Heisenberg spin model. It is shown that the pairwise energy variation calculated in terms of the multiple scattering formalism cannot be mapped onto a bilinear Heisenberg spin model for a simple non-collinear configuration of spins, even for the simplest case without considering the spin-orbit coupling. Some non-Heisenberg terms are induced by the spin-polarized host. However, for the particular case of the Fe bcc, we have shown that the exchange-coupling parameter related to the T_{2g} orbitals are Heisenberg-like and can be mapped onto a Heisenberg spin model even considering the non-collienar case. For that, we have rotated one atomic spin in a ferromagnetic background and have calculated, for each degree the exchange-coupling related to the T_{2g} and it showed very small dependence throughout the rotation.

4.3 Magnetism and ultrafast magnetization dynamics

In Paper **IV**, we have used the extended LKAG formalism able to calculate exchange-coupling parameters for non-collinear case to analyse the behavior of different Co structures, e.g. bcc, fcc and hcp crystals; as well as how the crystal behaves under Mn doping. Our results have shown interesting results where all crystal structures of Co are found to have and almost perfect Heisenberg behavior, by using the same set up previously described for Fe bcc, i.e. rotating one spin in a ferromagnetic background and analysing the exchange-coupling parameter dependence on the rotation. Having a Heisenberg behavior in this context means that one can have the correct description of the time evolution of the magnetic moments under the influence of a temperature-dependent laser pulse. In the other hand, for the same set up, Mn shows a strongly dependence on the rotation of one spin in a ferromagnetic background, revealing its strong non-Heisenberg behavior. Therefore, dopants of Mn in CoMn alloys drives the system to have a non-Heisenberg behavior as Mn scales into the system, although small amount of Mn is not

expected to brake this Heisenberg behavior. Later, the structural and magnetic properties of Co-rich CoMn alloys were calculated and compared with experimental data, which has shown good agreement with our theoretical findings. Lastly, the time-dependent behavior of the magnetism of Co in bcc, fcc and hcp structures together with the CoMn alloys were analysed after a laser pulse excitation. It was shown that the ultrafast magnetization dynamics strongly depends on the damping parameter and the concentration of Mn, due the Mn influence on the changing of the exchange-coupling parameter.

4.4 Implementation of the Dzyaloshinskii-Moriya interaction

In Paper **VI**, we have shown our implementation of a simple way to calculate the Dzyaloshinskii-Moriya interaction (DMI). As far as we know, it is the only method capable of calculating the DMI from a non-collinear magnetic configuration. There, we have performed calculations for 2D Mn systems on top of Ag(111) and Au(111), from nanostructures to monolayers. We have revealed that, for a collinear ferromagnetic configuration with the moments perpendicular to the surface plane, the same nanostructures show different DMI strengths and directions between the substrates. For a monolayer of Mn on top of Ag(111), the z direction of DMI is slightly stronger than the Mn monolayer on Au(111), although their plane components x and y are essentially the same. Concerning the strength, the Mn monolayer on Au(111) has a much stronger long-range behavior than on Ag(111), where the DMI drops to zero after a few Mn neighbors. These findings are in good agreement with the literature. Later, we extend the analysis to nanostructured systems, e.g. triangular trimers and hexagonal disks-like systems, with the latter being composed by a central atom and its six nearest neighbors in a fcc(111) surface lattice. Within the nanostructured systems, we have shown that the strength and direction does not change drastically from the monolayer to the nanostructure. Later, we have explored how the DMI vectors change when non-collinearity comes to be a factor. For that, we have allowed the magnetic moments to relax and find the ground state for each system and then calculated the DMI from these new magnetic configurations. Interestingly enough, our results show that due the complex role that spin and charge currents play in the system when the non-collinearity is present, both strength and directions can be different from the collinear case. These findings show, as seen for the J_{ij}'s, the importance of the non-collinear limit when dealing with exchange parameters. These new limit can strongly influence in dynamics properties and, therefore, could possibly be relevant for future development of technologies based on spintronics, for instance.

5. Outlook and perspectives

This thesis was focused in studying the exchange parameters from ab initio methods in order to explore new limits and improve the information given to modelling more complex systems, using Atomistic Spin Dynamics (ASD) methods, for example. These parameters are the exchange-coupling J_{ij} and the Dzyaloshinskii-Moriya interactions (DMI) that were extended to be understood under the light of new interpretations. The J_{ij} was split into orbital contributions showing the complexity of its individual contributions, while the DMI was extended to be calculated not only from a collinear magnetic configuration already done in the literature, but also from any non-collinear configuration, with the case where the ground state is non-collinear particularly studied here. It was also implemented a connection between the reciprocal space and the real space, made by calculating the energy dispersion from Bloch Spectral Function by performing a Fourier transformation of the real space Green function.

Among the studies that have used the implementation with which one is able to calculate the orbital contributions from J_{ij}, transition metals were investigated. The results showed that different orbitals, in case of cubic lattice, the T_{2g} and E_g, behave quite distinctly than the general trend. This gives new insights when designing new magnetic materials. Understanding how these particular orbitals behave under non-collinear configuration, also give us information whether some approximations are valid. The Heisenberg spin model can describe many dynamical magnetic properties and the mapping with these parameters is essential to a correct description of the experiments and to predict new phenomena. For instance, it was revealed the intriguing behavior of Fe bcc concerning to how each orbital, T_{2g} and E_g, contribute to the microscopic picture, being the former one mostly responsible to the formation of the Fermi surface and the long-range interaction (here, not only for Fe, but also the other studied $3d$ elements). It was also shown the Heisenberg behavior of Co fcc, bcc and hcp; and how the non-Heisenberg behavior of Mn influences dynamic and other magnetic properties in the CoMn alloys.

Lastly, still giving new insights for the modelling magnetic materials, we have shown the dependence of the DMI vectors strength and direction to not only different substrates, but more importantly, the dependence on the magnetic configuration. Here, we have studied triangular trimers of Cr on Au(111) and Mn on Au(111) and Ag(111), revealing the difference of the DMI vectors for these nanostructures between different substrates. Furthermore, we have shown the role of non-collinearity in the final DMI vectors that can highly impact in the properties of the spin dynamics of systems where the DMI plays

a crucial role, such as skyrmionic materials that are being highly studied due its technological potential. We believe that our studies can open up new windows where new limits are explored and the communication not only between theory and experiment, but also theory and theory are improved.

6. Sammanfattning på svenska

Sedan antiken, har magnetism som fenomen varit känt. Efter att först ha varit känt för sina mystiska egenskaper har magnetismen och magnetiska material lett oss till flera viktiga tekniska framsteg. Från applikationer i medicinska tillämpningar till datalagring har magnetismen en grundläggande roll och studierna inom området har utvecklats kraftigt motiverat av potentiella framtida tekniska tillämpningar. Som exempel har ett stort antal experimentella tekniker utvecklats för att kunna analysera magnetiska nanostrukturer och andra magnetiska material. Vi kan lyfta fram ett antal av dessa tekniker, såsom Spin-Polarized Scanning Tunnel Microscope (SP-STM) [1–10], Atomic Force Microscope (AFM) [13] och spektroskopi baserat på Röntgendikroism (XMCD). En annan viktig milstolpe för forskningen om magnetism är den teori som utvecklats av Hohenberg och Kohn, densitetsfunktionsteori (DFT) [16]. Med denna teori förbättrades möjligheten att genomföra precisa teoretiska undersökningar av material avsevärt.

Genom samarbetet mellan experimentalister och teoretiker kan teknologier utvecklas för att förbättra våra liv. Den nya och växande komplexiteten hos nya material ställer fortsatt höga krav på goda samarbeten mellan dessa grupper. För att hantera detta krävs en konstant förbättring av välkända metoder. Det finns många olika metoder som använder DFT för att beräkna den elektroniska strukturen för ett visst system. Särskilt här har vi arbetat för att förbättra den så kallade “Real Space Linear Muffin Tin Orbitals method within the Atomic Sphere Approximation” (RS-LMTO-ASA) [18–21], som löser egenvärdesproblemet som formuleras inom DFT i det reella rummet och som kan hantera icke-kollinär magnetism. När problemet löses i det reella rummet, är studier av nanostrukturer mindre kostsam jämfört med metoder som utvecklats för det reciproka rummet, såsom vanliga metoder baserade på planvågor. Det betyder att man kan hantera nanoskalade system, såsom en enda atom, öar eller nanostrukturerade material som adsorberas på en given yta utan att symmetrin blir ett problem. För dessa geometrier är material mer benägna att uppvisa icke-kollinär magnetisk ordning såsom magnetiskt grundtillstånd. Även om DFT-metoder är utformade för att vara effektiva, är de inte passande för att beskriva mesoskopiska effekter på grund av deras höga beräkningskostnader. För att komma till rätta med detta problem kan man använda flerskaliga metoder genom vilka man kan beräkna parametrar från DFT, som kan beskriva systemets övergripande beteende och använder dem för att parameterisera Hamiltonianer som sedan kan modellera speciella problem mer effektivit. När det gäller magnetiska system kan man använda sig

av Spinnhamiltonianer för att förutsäga viktiga egenskaper hos ett givet system, såsom grundtillstånd, fasövergångar (mellan faser som ferromagnetisk, anti-ferromagnetisk, paramagnetisk, skyrmionisk fas m.m.), kritiska temperaturer, effekter av externa magnetfält, systemets magnetiseringsdynamik, etc. Noggrannheten i dessa beräkningar är beroende av hur väl beskrivet systemet är av en Heisenberg-modell, eller annorlunda uttryckt, hur Heisenberg-likt ett system är. En effektiv bilinjär spinnväxelverkanshamiltonian kan innehålla tre parametrar: utbyteskopplingsparametern J_{ij}, Dzyaloshinskii-Moryia växelverkan $\vec{D}_{ij}$ och ett anisotropibidrag. I denna avhandling kommer vi att fokusera på de två första parvisa interaktionerna: utbyteskopplingsparametern J_{ij} och Dzyaloshinskii-Moryia växelverkan D_{ij} [22, 23]. DMI för vissa strukturer kan ses i Fig. 6.1.

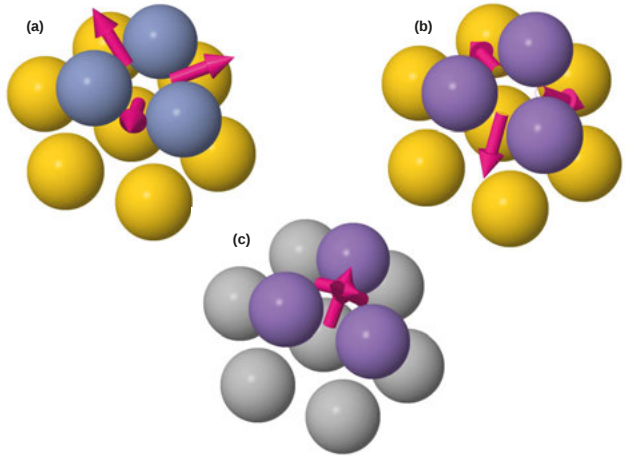

Figur 6.1. Schematisk representation av en triangulär trimer av: (a) Cr på Au (111), (b) Mn på Au (111) och (c) Mn på Ag (111) fcc ytor. De rosa pilarna betecknar normaliserad DMI-riktning, vid kolinär magnetisk konfiguration (ferromagnetisk med magnetiska moment vinkelrätt mot ytan), och de står mellan två atomer som interaktionen motsvarar.

En annan mycket användbar tillämpning av den så kallade Heisenberghamiltonianen är att beräkna det effektiva magnetfältet i systemet och studera dess magnetodynamiska egenskaper [24–26]. Särskilt inom sektorn för informationsteknologi görs kraftfulla ansträngningar för att förbättra hur snabbt och effektivt information kan lagras. Ett nytt och lovande forskningsområde med hög relevans för det är spinntronik. Spinntronik är ett brett fält och använder magntiska moments dynamk för tekniska tillämpningar. Inom detta område har ett ämne fått stor uppmärksamhet på senare tid: skyrmioner. Skyrmioner inom magnetismen är föremål som uppvisar en topologiskt skyddad magnetisk konfiguration med kvasipartikelegenskaper, vilket har stor användbarhet

i informationsteknik på grund av dess rörlighet och stabilitet [34–42]. Studier av dessa material kan genomföras med hjälp av en kombination av textit ab initio metoder, såsom RS-LMTO-ASA, och magnetiseringsdynamikmetoder [24–33]. I den här avhandlingen har vi noggrant undersökt utbytesparametrarna genom att ingående studera vilka faktorer som är inblandade i beräkningarna av dem. Vi har infört nya funktionaliteter i RS-LMTO-ASA-metoden vilket gör att vi kan studera dessa parametrar ur nya perspektiv. Det kommer att berika den redan kända kunskapen om magnetism i allmänhet och magnetiska växelverkningar i synnerhet och därmed bidra till ytterligare framtida forskningsmöjligheter.

7. Resumo em português

Desde os tempos antigos, datados de séculos A.C., o magnetismo é conhecido. Primeiramente pelas suas propriedades místicas, o fenômeno do magnetismo tem nos levado a progressos tecnológicos importantes. De aplicações em medicina a tecnologia da informação, o magnetismo tem um papel fundamental e seu estudo tem sido importante para futuras aplicações tecnológicas. Dentre esses estudos, técnicas experimentais têm sido amplamente desenvolvidas no que diz respeito ao estudo de nanoestruturas. Podemos destacar algumas como *Spin-Polarized Scanning Tunneling Microscope* (SP-STM) [1–10], *Atomic Force Microscope* (AFM) [13] e *X-ray Magnetic Circular Dichroism* (XMCD). Outro importante avanço foi o desenvolvimento da teoria do funcional da densidade (DFT) [16], por Hohenberg e Kohn. Esta teoria foi fundamental para o estudo de materiais e suas propriedades na física do estado sólido.

Através da cooperação entre teóricos e experimentais, a tecnologia pode progredir para melhorar nossa qualidade de vida. Essa comunicação tem sido cada vez mais desafiada pelo aumento da complexidade de novos materias. Com isso, é preciso haver um constante melhoramento de métodos teóricos e experimentais. Existem diferentes métodos na literatura que usam DFT para calcular a estrutura eletrônica de um dado sistema. Neste trabalho, aperfeiçoamos o método *real space linear muffin-tin orbitals atomic sphere approximation* (RS-LMTO-ASA) [18–21], o qual resolve o problema de auto-valores no espaço real e também pode lidar com magnetismo não-colinear. Com o problema sendo resolvido no espaço real, o estudo de nanoestruturas passa a ser menos custoso computacionalmente, comparado com métodos desenvolvidos no espaço recíproco, tais como os métodos baseados em ondas planas. Isto significa que é possível lidar com sistemas em nano-escala, como por exemplo um único átomo, ilhas ou materiais nanoestruturados adsorvidos em uma superfície, justamente onde os sistemas estão propícios a apresentarem o magnetismo não-colinear como o possível estado fundamental. Embora métodos baseados no DFT sejam projetados para serem eficientes, eles não são adequados para descrever efeitos mesoscópicos devido ao alto custo computacional. A fim de superar este problema, pode-se empregar métodos *multi-scale* onde usamos parâmetros calculados diretamente de métodos que usam o DFT, os quais dão informações gerais sobre o sistema estudado. Posteriormente, usamos estes parâmetros em Hamiltonians que podem modelar problemas pontualmente com mais efetividade e menos custo computacional. No que diz respeito a problemas envolvendo magnetismo, podemos fazer uso

das *spin-Hamiltonians* para prever características importantes de um dado sistema, como por exemplo o estado fundamental, transição de fases (entre fases como fase ferromagnética e anti-ferromagnética, paramagnética, fase de skyrmions, etc.), temperatura crítica, efeito de um campo magnético externo, a dinâmica magnética do sistema, etc. A precisão destes cálculos está ligada diretamente a proximidade do sistema e como a Hamiltoniana é representada, em outras palavras, o quanto o sistema é *Heisenberg-like*. Uma Hamiltoniana bi-linear geralmente conta com três parâmetros: o parâmetro de acoplamento e troca J_{ij}, a interação Dzyaloshinskii-Moryia $\vec{D}_{ij}$ e um termo que representa a anisotropia do sistema. Neste trabalho, nós iremos focar nas duas interações emparelhadas: o parâmetro de acoplamento e troca, e a interação Dzyaloshinskii-Moryia [22, 23].

Outro importante uso da Hamiltoniana de Heisenberg (Hamiltoniana bilinear de spin) é o cálculo do campo magnético efetivo sofrido pelo sistema e através disto calcular suas propriedades magnéticas dinâmicas [24–33]. Particularmente, no que diz respeito a tecnologia da informação, esforços estão sendo aplicados na direção de melhorar a velocidade em que a informação é transmitidas e transformada, assim como aprimorar a capacidade de armazenamento de dados. Dentro deste campo, um assunto vem ganhando bastante atenção ultimamente: skyrmions. Skyrmions são, no campo de magnetismo, estruturas magnéticas topologicamentes protegidas com características de quase-partículas, o que oferece um grande potencial de aplicabilidade em tecnologia da informação devido a sua mobilidade e tamanho [34–42]. O estudo dessas estruturas pode ser feito com uma boa comunicação entre métodos *ab initio*, como o RS-LMTO-ASA, e métodos de dinâmicas de spin [24–26]. Nesta tese, nós investigamos mais profundamente os parâmetros calculados de métodos *ab initio* a fim de aprimorar as propriedades calculadas através das Hamiltonianas de spin. Nós implementamos novas ferramentas no método RS-LMTO-ASA que nos possibilita estudar este parâmetros através de novas perspectivas, as quais nós acreditamos que irá melhorar as informações já conhecidas na literatura e possivelmente assistir futuramente em novas possibilidades de pesquisa.

Acknowledgement

This work would never be possible to be done without the help of a great support from people around me. Thankfully, this experience between two countries has lead me to meet many of those great people. Both inside and outside the academia, friends and family have been crucial to survive these years of battle. Here, I would like to give my many thanks to a special group that has made this path more enjoyable and fruitful.

- To my family. I am a lucky guy to have a big supportive family. To my parents, Lucilene Cardias and Rômulo Corinto, my big thanks for all the support throughout all those 28 years of my life. Many thanks also to my aunt Lucibela Cardias and uncle Ilmar Lopes for the times that I needed extra support and you were always there. Special thanks to my little sister for being always by my side, always showing different and positive perspectives of life. My cousins Pablo and Paola Soares, you are a extremely important pillar in my life. I love you all.
- To my supervisors Prof. Ângela Klautau, Prof. Olle Eriksson, Dr. Anders Bergman and Dr. Attila Szilva. Your patience and uncountable discussion during this time were essential. I can not measure how grateful I am. Thanks for believing and investing in me.
- My dear colleagues and friends that I have made in Uppsala University, Yaroslav Kvashnin, Danny Thonig, Jonathan Chico and Konstantinos Koumpouras. The valuable discussions about physics and life have made my day, everyday. Thank you.
- To my brazilian colleagues and friends, my big thanks. Manoel Neto, Marcelo Ribeiro, Alessandra Braga, Riis Rhavia, Carol Benone, thank you all for sharing the good moments of our warm Belém, and to Larissa Pimentel, from Belém to Europe, thank you for the valuable conversations. Special thanks do Débora Rodrigues. No words for all the support I received from you.
- To all the friends I made somehow in Uppsala, thank you Luimar Correa, Filipe Mussini, Giane Damas, Mailing Bewanger, Andre Lobato, Daniele Braga, Mauricio Antunes and Beatrice Nybert; thank you all for keeping me warm with lots of good laughs during the rough winter.
- The quote "If I have seen further, it is by standing on the shoulders of Giants" literally describes my last thanks. To my grandfather, Corinto Silva de Almeida. The times when you used to pick me up from elementary school bringing me home on your shoulders, your stories, your teachings and your love for me will never be forgotten.

Appendix A.
LMTO-ASA formalism

A.1 Introduction

Here, we will solve the Kohn-Sham equation through a linear method, which uses energy independent basis function. The linear muffin-tin orbital - atomic sphere approximation (LMTO-ASA) method is an example of a linear method. The LMTO formalism was initially developed in the canonic basis, however, O. K Andersen [45] has shown that the LMTO formalism can be described as a function of other basis set, e.g. canonical basis, orthogonal basis and the most localized basis called tight-binding (TB). In this way, one has the freedom to choose the most appropriate basis to be used for a given study. In our case, there are two basis set that make our calculations easier: the orthogonal basis, where the wave functions are orthogonal between themselves, and the localized TB basis. In this appendix, the specifics aspects of the TB and orthogonal basis will be shown as well as how they relate with each other. A more general formulation about the canonical basis and the complete description of how to change to a generic basis can be found in the literature [51, 72].

A.2 The eigenvalue problem

As seen in the Chapter 2, DFT simplifies the many-body problem, formulating it into a problem of one electron moving under the effect of an effective potential. For this new reformulation, one needs to solve the Kohn-Sham equation, which in this appendix will be called a Schrödinger-like equation. To start, one can write the wave function ψ_j as a linear combination of basis χ_i, energy independent basis functions

$$\psi_j = \sum_i \chi_i u_{i,j}, \tag{A.1}$$

where $u_{i,j}$ are the expansion coefficients. Substituting the expansion terms in the Schrödinger-like equation, the following eigenvalue problem needs to be solved

$$(\hat{H} - EO)u = 0, \tag{A.2}$$

with $\hat{H}$ being the Hamiltonian matrix and O the overlap matrix, both independent in energy and described by

$$\hat{H}_{ji} = \left\langle \chi_j \left| (-\nabla^2 + V) \right| \chi_i \right\rangle \tag{A.3}$$

and

$$O_{ji} = \left\langle \chi_j | \chi_i \right\rangle . \tag{A.4}$$

In order to simplify the calculation, a few approximations are done. One is the so called Atomic Sphere Approximation (ASA), where the crystal is considered filled by spheres centred in each atomic site R and neglect the interstitials and overlap regions. The radius a of each sphere is chosen in such a way that the summation of the volume occupied by the spheres is equal to the volume occupied by the atoms in the material. In the particular case of a material constituted by only one atom, this radius is called Wigner-Seitz radius. It is noteworthy to say that this approximation is appropriate for densely packed materials. Another valid approximation concerns the potential symmetry. Here, for each sphere centred in the site R, the potential V_R is considered spherically symmetric.

$$V = \sum_R V_R. \tag{A.5}$$

A.3 Development of the LMTO-ASA formalism in the canonical basis

Inside the LMTO-ASA formalism, the χ_i basis must be chosen in a convenient way in order to obtain the Hamiltonian matrix, Eqn. A.3, and a overlap matrix, Eqn. A.4, with a given number of functions that are, at least, the minimum number of functions able to describe the system. In case of transition metals, the object of our study, one can choose 9 orbitals per site, being 1 s, 3 p and 5 d. In order to create one basis with these characteristics, one considers an isolated sphere of radius a, centred on the site R. Hence, a symmetric muffin-tin potential is taken inside the sphere and constant outside of it. Inside the sphere or radius a, where the spherical symmetric potential is situated, the Schrödinger-like equation solution must be differentiable and continuous in all space towards the outside of the sphere. Also, it is considered that the kinetic energy outside the radius a, in the interstitial region, is null. This approximation is convenient in the ASA approximation, since this region is not taken into consideration. Hence, outside the sphere of radius R, the solution for the Schrödinger-like equation is given as

$$K_{RL}(r_R) = \left| \frac{\vec{r_R}}{a} \right|^{-l-1} Y_L(\hat{r}_R), \tag{A.6}$$

with the $\vec{r}_R = \vec{r} - \vec{R}$, $Y_L(L = l,m)$ being the spherical harmonics and a is a factor that has to be chosen appropriately. Usually, the value of a is chosen as the Wigner-Seitz radius of the studied material. Lastly, the values for l are related to the orbitals s, p and d; being $l = 1$, 2 and 3, respectively.

Taking into account that the ASA approximation is a group of juxtaposed spheres centred on each atomic site, with a spherical symmetric potential inside the sphere, one needs a process that describes the system correctly. This process consists of substituting part of the K_{RL} function inside the spheres, centred on the sites $\vec{R} \neq \vec{R}'$, by functions that are solutions of the Schrödinger-like equation, so that the logarithmic derivatives in the sphere boundary can be continuous. These auxiliary functions are called envelope functions. They have the objective to establish the boundary conditions that has to be obeyed by the solution of the Schrödinger-like equation inside the spheres centred in $\vec{R}'$. In the canonic basis, the envelope functions, before defined by Eqn. A.6, is now written as

$$K_{RL}(\vec{r}_R) = k_{RL}(r_R)Y_L(\hat{r}_R). \tag{A.7}$$

In this equation, the radius part is given by the $k_{RL}(r_R)$ and it is written as

$$k_{RL}(r_R) = \left(\frac{r_R}{a}\right)^{-l-1}. \tag{A.8}$$

In order to obtain the functions χ^0_{RL} in the canonical basis, one needs to substitute part of the envelope solution, Eqn. A.7 defined on the spheres R', by functions related to the solution of the Schrödinger-like equation inside the spheres, given a spherical symmetric potential, which is obtained self-consistently. These functions are orthogonal with respect to the core levels, in the region around the site $\vec{R}'$, being then a good approximation for the solution of the problem in this region. Note that the substitution process must consider the continuity and differentiability conditions on the sphere limits. This process is assisted by the envelope functions and it is known by augmentation. In order to realize this process, one needs to expand the envelope function around the sites $\vec{R}'$, since the Schrödinger-like equation has well defined solution around $\vec{R}'$. For such expansion, one needs to take part of the K_{RL} that extends itself on the centred spheres $R \neq R'$ (defined by χ^0_{RL}) and write it as an expansion around the regular solutions to the Laplace equations in the origin and centred in $R'L'$, described by

$$K^0_{RL} = -\sum_{R'L'} J^0_{R'l'}(r_{R'})S^0_{R'L',RL}, \quad r > s, \tag{A.9}$$

with $J^0_{R'l'}(r'_R)$ being null outside the spheres of centred in R' and radius s, described inside by

$$J^0_{R'l'}(r_{R'}) = \left|\frac{\vec{r_{R'}}}{a}\right|^{l'} \frac{1}{2(2l'+1)} Y'_L(r'_R). \tag{A.10}$$

In the Eqn. A.9, the coefficients $S^0_{R'L',RL}$ exist only between $\vec{R}$ and $\vec{R}'$, being null for $R = R'$. The structure matrix in the canonical basis is called S^0 and its elements are the expansion coefficients of the K_{RL} function around $\vec{R}'$, given by

$$S^0_{R'L',RL} = \frac{1}{(4\pi)^{1/2}} G_{l'm',lm} \left|\frac{\vec{R}-\vec{R}'}{a}\right|^{-l'-l-1} Y^*_{l'+1,m'-m}(\vec{R}-\vec{R}') \quad , \tag{A.11}$$

where $G_{l'm',lm}$ is written as

$$G_{l'm',lm} = (-1)^{l+m+1} \left[\frac{(2l'+1)(2l+1)(l+l'+m'-m)!(l+l'-m'+m)!}{(2l'+2l+1)(l'-m')!(l'-m')!(l+m)!(l-m)!}\right]^{1/2}. \tag{A.12}$$

Now the envelope function centred on the site $\vec{R}$ and defined in all the space is defined as

$$K^\infty_{RL} = k_{Rl}(r_R) Y_L(\hat{r}_R) - \sum_{R'L'} j^0_{R'l'}(r_{R'}) Y_{L'}(\hat{r}_{R'}) S^0_{R'L',RL}, \tag{A.13}$$

where

$$k_{Rl}(r_R) = \left|\frac{\vec{r_R}}{a}\right|^{-l-1}, \tag{A.14}$$

and

$$j^0_{R'l'}(r_{R'}) = \left|\frac{\vec{r_{R'}}}{a}\right|^{l'} \frac{1}{2(2l'+1)}. \tag{A.15}$$

If one uses the Dirac notation, the envelope function is written as

$$|K\rangle^\infty = |\,K\rangle - \left|J^0\right\rangle S^0. \tag{A.16}$$

Once the envelope function K^∞_{RL} is calculated, we can proceed with the augmentation process. For this second part, one must substitute the envelope function inside the sphere by solutions of the Schrödinger-like for a spherically symmetric potential, always verifying if the boundary conditions established by the envelope functions are being satisfied. In order to do that, one needs to find the radial solution of the Schrödinger-like equation for a spherically symmetric potential inside of each sphere centred at R, in order to obtain the

normalized solutions $\varphi_{RL}(r,E)$. Taking $\varphi_{RL}(r,E)$ and its derivative calculated for $E = E_{\nu,Rl}$, we have

$$\varphi_{RL}(r) = \varphi_{RL}(r,E_\nu) \tag{A.17}$$

and

$$\dot{\varphi}_{RL}(r) = \frac{\partial}{\partial E}\varphi_{RL}(r,E)|_{E=E_\nu}. \tag{A.18}$$

In this way, one is able to write the basis energy-independent. Then, the function $\chi^{0\infty}_{RL}$ is taken in all the space and is written as a linear combination of the radial solutions and its derivatives, Eqns. A.17 and A.18, respectively. Then

$$\chi^{0\infty}_{RL}(\vec{r}_R) = \varphi_{Rl}(r_R)Y_L(\hat{r}_R) + \sum_{R'L'} \dot{\varphi}^0_{R'l'}(r_{R'})Y_{L'}(\hat{r}_{R'})h^0_{R'L',RL}, \tag{A.19}$$

and using that

$$\dot{\varphi}^0_{R'l'}(r_{R'}) = \dot{\varphi}_{R'l'}(r_R) + \sum_{R'L'} \varphi_{R'l'}(r_R)o^0_{R'l'}, \tag{A.20}$$

Using A.20 in A.19

$$\chi^{0\infty}_{RL}(\vec{r}_R) = \varphi_{Rl}(r_R)Y_L(\hat{r}_R) + \sum_{R'L'} \left[\dot{\varphi}_{R'l'}(r_R) + \varphi_{R'l'}(r_R)o^0_{R'l'}\right] Y_{L'}(\hat{r}_{R'})h^0_{R'L',RL}, \tag{A.21}$$

where the functions φ_{Rl} and $\dot{\varphi}_{Rl}$ are defined only to the sphere centred in $\vec{R}$ and the index ∞ says that the function is defined in all space.

Rewriting the functions A.19, A.20 and A.21 in the vectorial (Dirac) notation

$$\left|\chi^0\right\rangle^\infty = |\varphi\rangle + \left|\dot{\varphi}^0\right\rangle h^0, \tag{A.22}$$

with

$$\left|\dot{\varphi}^0\right\rangle = |\dot{\varphi}\rangle + |\varphi\rangle\, o^0 \tag{A.23}$$

or

$$\left|\chi^0\right\rangle^\infty = |\varphi\rangle\,(1 + o^0h^0) + |\dot{\varphi}\rangle\, h^0, \tag{A.24}$$

where $|\varphi\rangle$, $\left|\dot{\varphi}^0\right\rangle$, $\left|\chi^0\right\rangle^\infty$, etc. are the vectors of components $|\varphi_{RL}\rangle$, etc. and h^0 and o^0 are matrices. In this notation, the angular parts are included in the spherical harmonics around the site $\vec{R}$ and normalized to unity.

The calculation of the matrices h^0 and o^0 is done connecting the radial solutions of the envelope function, $k_{Rl}(r)$ and $j^0_{Rl}(r)$, to a linear combination of $\varphi_{Rl}(r)$ and $\dot{\varphi}_{Rl}(r)$ in such way that these functions fall on top of each other in the sphere boundary $r = s$ [72]. Doing this, the values for h^0 and o^0 can be obtained.

$$h^0 = \left[-\frac{W(k,\varphi)}{W(k,\dot{\varphi}^0)} + \left(\frac{2}{a}\right)^{1/2} W(j^0,\varphi) S^0 W(j^0,\varphi) \left(\frac{2}{a}\right)^{1/2} \right] \tag{A.25}$$

and

$$o^0 = -\frac{W(j^0,\dot{\varphi})}{W(j^0,\varphi)}. \tag{A.26}$$

Here, $W(a,b)$ are diagonal matrices called Wronskian of a and b, described as

$$W(a,b) = s^2[a(s)b'(s) - a'(s)b(s)], \tag{A.27}$$

where $f(s)$ is the function $f(r)$ in $r = s$ and $f'(s)$ is its derivative with respect to r in $r = s$. In these expressions, the indexes RL are not presented. The coefficient h^0 is a matrix with elements $h^0_{RL,R',L'}$ and o^0 is a diagonal matrix with elements o^0_{RL}.

With the elements h^0 and o^0 calculated, the canonical basis is finally done.

In the LMTO-ASA formalism, is usual to write the coefficient h^0 of the basis function in terms that are potential dependent and potential independent. Therefore, redefining h^0 using the parameters Δ^0 and C^0

$$h^0_{RL,R'L'} = (C^0_{Rl} - E_{\nu Rl})\delta_{R,R'}\delta_{L,L'} + \Delta^{0\frac{1}{2}}_{Rl} S^0_{RL,R'L'} \Delta^{0\frac{1}{2}}_{R'l'}, \tag{A.28}$$

with

$$C^0_{Rl} = E_{\nu Rl} - \frac{W(k_{Rl},\varphi_{Rl})}{W(k_{Rl},\dot{\varphi}_{Rl})} \tag{A.29}$$

and

$$\Delta^{0\frac{1}{2}}_{Rl} = \left(\frac{2}{a}\right)^{1/2} W(j^0_{Rl},\varphi_{Rl}). \tag{A.30}$$

Now it is possible to define the Hamiltonian matrix H^0 and the overlap matrix O^0, in the canonical basis, as

$$H^0 =^{\infty} \left\langle \chi^0 \right| -\nabla^2 + V \left| \chi^0 \right\rangle^{\infty}, \tag{A.31}$$

and

$$O^0 =^{\infty} \left\langle \chi^0 | \chi^0 \right\rangle^{\infty}, \tag{A.32}$$

respectively.

Using $\left|\chi^0\right\rangle^{\infty}$ in the Eqns. A.31 and A.32, and the properties of the functions H^0 and O^0 in terms of h^0 and o^0, then

$$H^0 = h^0 + (o^0 h^0)^{\dagger} h^0 + E_{\nu} O^0, \tag{A.33}$$

and

$$O^0 = 1 + o^0 h^0 + (o^0 h^0)^\dagger + (o^0 h^0)^\dagger o^0 h^0. \tag{A.34}$$

Note that small terms, of the order of $(h^0 + ph^0)$, with $p_{RL} = \left|\dot{\varphi}^2_{RL}\right\rangle$, where not taken into consideration. So, using H^0 and O^0, one can write the secular equation for the LMTO

$$\left(H^0 - E_j O^0\right) u^0_j = 0. \tag{A.35}$$

Solving this equation, one can calculate the eigenvalues for the particular case of the canonical basis. At first sight, the problem would be solved, since the solution of Eqns. A.35 determines the electronic structure of the material. However, in the direct space, this procedure is only convenient if the Hamiltonian matrix is localized, which is not guaranteed in the canonical basis. The structure matrix S^0 decays very slowly with the distance, extending itself through many neighbor shells, being then non-local. This is enough to conclude that the Hamiltonian in the canonical basis will not be localized either. Therefore, more basis transformations are needed in order to obtain a better basis for our problem.

A.4 Generic basis

It is known that the LMTO-ASA formalism allows us to change the problem basis in order to find a proper one. So, firstly, one can generalize the representation in a way that the envelope function tail can be expanded in terms of one regular function J^0 and a irregular function K, having then

$$\left|J^G\right\rangle = \left|J^0\right\rangle - |K\rangle\, Q^G, \tag{A.36}$$

where Q^G is a diagonal matrix that dictates the mix between the irregular functions $K_{R'L'}$ with the regular functions $J^0_{R'L'}$. The envelope function would be then written as

$$\left|K^G\right\rangle^\infty = |K\rangle - \left|J^G\right\rangle S^G. \tag{A.37}$$

It is possible to show [51] that the structure matrix, in this representation, is given by

$$S^G = S^0(1 - Q^G S^0)^{-1}. \tag{A.38}$$

Then, the envelope functions of the different basis are related with each other in the following manner

$$\left|K^G\right\rangle^\infty = |K\rangle\left(1 + Q^G S^G\right) - \left|J^0\right\rangle S^G. \tag{A.39}$$

In this representation, the structure matrix S^G is connected with the material electronic structure as well as depend on the potential on the spheres through the parameter Q^G.

Analogously with what was done for the canonical basis, it is possible to define a function $\left|\chi^G\right\rangle^\infty$ in the general representation and as a function of h^G and o^G, such as

$$\left|\chi^G\right\rangle^\infty = |\varphi\rangle\,(1+o^G h^G)+|\dot{\varphi}\rangle\,h^G. \tag{A.40}$$

and

$$\left|\dot{\varphi}^G\right\rangle = |\dot{\varphi}\rangle + |\varphi\rangle\,o^G. \tag{A.41}$$

or in the following manner

$$\left|\chi^G\right\rangle^\infty = |\varphi\rangle\,(1+o^G h^G)+|\dot{\varphi}\rangle\,h^G. \tag{A.42}$$

The parameters h^G and o^G are determined by the augment process. Hence, we have

$$h^G = -\frac{W(k,\varphi)}{W(k,\dot{\varphi}^G)} + \left(\frac{2}{a}\right)^{1/2} W(j^G,\varphi) S^G W(j^G,\varphi) \left(\frac{2}{a}\right)^{1/2} \tag{A.43}$$

and

$$o^G = -\frac{W(j^G,\dot{\varphi})}{W(j^G,\varphi)} = -\frac{W(j^0,\dot{\varphi}) - W(k,\dot{\varphi})Q^G}{W(j^0,\varphi) - W(k,\varphi)Q^G}, \tag{A.44}$$

where o^G is a diagonal matrix with elements o^G_{Rl} e h^G_{Rl} is a matrix with elements $h^G_{RL,R'L'}$(note that the indexes Rlm were suppressed). So, using the expression $\left|\chi^G\right\rangle^\infty$ in terms of the matrices h^G and o^G, it is possible to define the Hamiltonian H^G matrix and the overlap O^G matrix in the generic basis

$$H^G =^\infty \left\langle \chi^G \right| -\nabla^2 + V \left| \chi^G \right\rangle^\infty = h^G + (o^G h^G)^\dagger h^G + E_v O^G, \tag{A.45}$$

and

$$O^G =^\infty \left\langle \chi^G | \chi^G \right\rangle^\infty = 1 + o^G h^G + (o^G h^G)^\dagger + (o^G h^G)^\dagger o^G h^G. \tag{A.46}$$

A.5 Tight-binding basis - the localized basis

Since we have the freedom of taking a parameter of any mixture Q^G, then one can take a parameter in order to make the basis as localized as it can be, in such way that only the interaction between the first neighbors are sufficient to the correct description of the problem. This localized Hamiltonian matrix

enables the use of the recursion method, which is efficient when dealing with problems in the real space.

As mentioned before, the structure matrix, given by $S^G = S^0(1 - Q^G S^0)^{-1}$, also depends on the mixture parameter Q^G. The values for the mixture parameters were calculated by O. K. Andersen and O. Jepsen [51, 62]. The obtained values are structure independent and the structure matrix decays exponentially with the distance between the atoms. The values are

$$\bar{Q}_s = 0,3485, \tag{A.47}$$

$$\bar{Q}_p = 0,05303, \tag{A.48}$$

$$\bar{Q}_d = 0,010714 \tag{A.49}$$

and

$$\bar{Q}_l = 0, \;\; l > 2\,. \tag{A.50}$$

where $Q^G = \bar{Q}$ are the parameters in the TB basis. In the TB basis, the eigenvalue equation is described by

$$\left(\bar{H} - \bar{E}\bar{O}\right)\bar{u} = 0. \tag{A.51}$$

Substituting h^G and o^G for $\bar{h}$ and $\bar{o}$, respectively, in the Eqns. A.45 and A.46, it is obtained

$$\left(\bar{H} - \bar{E}\bar{O}\right)\bar{u} = \left[\bar{h} + \bar{h}^{\dagger}\bar{o}^{\dagger}\bar{h} + E_{\nu}\bar{O} - E\bar{O}\right]\bar{u} = 0\,, \tag{A.52}$$

A.6 The orthogonal basis

It is possible to recover the orthogonal basis by forcing the overlap matrix to be the identity matrix. For that, one just needs to have $o^G = 0$. Note that this basis is interesting to deal with, since it makes it simple to obtain the eigenvectors and eigenvalues of the equation $(H^G - EO^G)u^G = 0$. In the orthogonal basis notation, the upper indexes are suppressed. The Hamiltonian matrix in the orthogonal basis can be written as

$$H = h + E_{\nu}. \tag{A.53}$$

Therefore, the eigenvalue equations is written as the following manner

$$Hu = Eu, \tag{A.54}$$

or

$$(h + E_{\nu})\,u = Eu. \tag{A.55}$$

Consequently

$$h = E - E_\nu. \tag{A.56}$$

The Hamiltonian H can be written as a function of the potential parameters in the orthogonal basis as

$$H = C + \Delta^{1/2} S \Delta^{1/2}, \tag{A.57}$$

where

$$C = E_\nu - \frac{W(k,\varphi)}{W(k,\dot{\varphi})} \tag{A.58}$$

and

$$\Delta^{1/2} = \left(\frac{2}{a}\right)^{1/2} W(j,\varphi). \tag{A.59}$$

For the structure matrix S

$$S = S^0 \left(1 - QS^0\right)^{-1}, \tag{A.60}$$

where the term Q is obtained by choosing $o^G = 0$

$$Q = \frac{W(j,\dot{\varphi})}{W(k,\varphi)}. \tag{A.61}$$

The basis functions in the orthogonal basis are written as

$$|\chi\rangle^\infty = |\varphi\rangle + |\dot{\varphi}\rangle h. \tag{A.62}$$

Then, by doing $h = H - E_\nu$, one can have

$$|\chi\rangle^\infty = |\varphi\rangle + |\dot{\varphi}\rangle (H - E_\nu). \tag{A.63}$$

Now, writing the this equation in terms of the eigenvalues of H, one can reach

$$|\chi\rangle^\infty = |\varphi\rangle + |\dot{\varphi}\rangle (E - E_\nu). \tag{A.64}$$

Remember that in the LMTO-ASA formalism, the functions written in the orthogonal basis are given by Taylor expansion up to the first order in energy of the partial wave $|\varphi(E,r)\rangle$ around the energy E_ν.

A.7 Orthogonal representation of the Hamiltonian matrix as function of tight-binding representation parameters

It was shown so far that both the orthogonal and the TB basis simplify the calculations in the real space. The former one makes the problems to be simpler

and the latter one enables the utilization of the recursion method. However, in order to obtain one orthogonal Hamiltonian as a function of the potential parameters in the TB representation, one needs to find proper approximations that facilitates the process.

The Hamiltonian described by $H = h + E_\nu$ can be written in terms of the general basis in the following manner

$$h = h^G \left(1 + o^G h^G\right)^{-1}. \tag{A.65}$$

Note that this relationship is valid for any basis $\left|\chi^G\right\rangle^\infty$. Therefore, it is possible to represent the orthogonal basis Hamiltonian in terms of the TB parameters as

$$H = E_\nu + \bar{h}\left(1 + \bar{o}\bar{h}\right)^{-1}. \tag{A.66}$$

Taking the values for $\bar{o}\bar{h}$ very small, one can expand $(1+\bar{o}\bar{h})^{-1}$ in a power series of $\bar{o}\bar{h}$, and then

$$H = E_\nu + \bar{h} - \bar{h}\bar{o}\bar{h} + \bar{h}\bar{o}\bar{h}\bar{o}\bar{h} - ..., \tag{A.67}$$

where $\bar{h}$ is a hermitian matrix written as a function of the TB parameters and is described as

$$\bar{h} = \bar{C} - E_\nu + \bar{\Delta}^{1/2}\bar{S}\bar{\Delta}^{1/2}. \tag{A.68}$$

In this representation, $\bar{o}$, $\bar{C}$ and $\bar{\Delta}$ are the potential parameters in the TB basis and $\bar{S}$ is the structure matrix, also in TB basis. Taking the expansion up to the first order in $(E - E_\nu)$, the Hamiltonian is then written as

$$H^{(1)} \approx E_\nu + \bar{h} = \bar{C} + \bar{\Delta}^{1/2}\bar{S}\bar{\Delta}^{1/2}. \tag{A.69}$$

And if it is used up to the second order

$$H^{(2)} = H^{(1)} - \bar{h}\bar{o}\bar{h}, \tag{A.70}$$

where $H^{(1)}$ is the first order Hamiltonian. For a good description of the occupied bands of the s, p and d orbitals, the first order Hamiltonian is typically enough. However, if one wants a better description of the unoccupied states of these bands, it is necessary to include the terms of the second order expansion, i.e. the $\bar{h}\bar{o}\bar{h}$ terms. For the accurate description of the properties, such as magnetic moment, the addition of the second order term does not affect the results significantly.

In the real space, inside the RS-LMTO-ASA formalism, one must use the orthogonal representation for the Hamiltonian in terms of the TB potential parameters $\bar{C}$, $\bar{\Delta}$ and $\bar{S}$, given by

$$\bar{C} = E_\nu - \frac{W(k,\varphi)}{W(k,\dot{\varphi})}, \tag{A.71}$$

$$\bar{\Delta}^{1/2} = \left(\frac{2}{a}\right)^{1/2} W(\bar{j}, \varphi) \,, \tag{A.72}$$

and

$$\bar{S} = S^0 \left(1 - \bar{Q} S^0\right)^{-1} . \tag{A.73}$$

The relationship between the parameters of a more localized basis and the orthogonal basis is described as

$$\frac{\bar{\Delta}^{1/2}}{\Delta^{1/2}} = \left[1 - \left(Q - \bar{Q}\right) \frac{C - E_v}{\Delta}\right] = \frac{\bar{C} - E_v}{C - E_v}. \tag{A.74}$$

The calculation of the Hamiltonian H, represented as a function of the TB parameters, can be divided in two distinct parts. One depends on the potential of each sphere and obtaining the parameters $\bar{C}$ and $\bar{\Delta}$. The second part depends on the structure of the material and the calculation of the structure matrix $\bar{S}$ and does not depend on the potential.

Appendix B.
The Recursion Method

In this appendix, the recursion method and the Beer-Pettifor terminator used in the RS-LMTO-ASA method will be described. It has been shown that inside the RS-LMTO-ASA method, one can write the Hamiltonian in a orthogonal basis in terms of the TB parameters. The obtained Hamiltonian is a sparse matrix $9N$x$9N$, where N is the number of atoms considered and 9 is the number of the considered orbitals. Given the matrix dimension, the eigenvalue problem is impracticable to solve. Therefore, a method that makes the problem solvable is needed. This method is the recursion method developed by R. Haydock [52]. The goal of the recursion method is to shape the regular problem Hamiltonian into a tridiagonal (Jacobi matrix) Hamiltonian matrix, through a basis change.

Since the Hamiltonian will be tridiagonal, each element $|u_n\rangle$ must only interact with the previous and posterior elements $|u_{n-1}\rangle$ and $|u_{n+1}\rangle$, respectively. A recursion relationship can the be identified as

$$H|u_n\rangle = a_n|u_n\rangle + b_{n+1}|u_{n+1}\rangle + b_n|u_{n-1}\rangle, \tag{B.1}$$

where H is the Hamiltonian in the orthogonal basis written as a function of the TB parameters and $\{a_n, b_n\}$ are the coefficients that describe the interaction of $|u_n\rangle$ with $|u_{n-1}\rangle$ and $|u_{n+1}\rangle$. In order to obtain the coefficients a_n and b_n, a arbitrary orbital $|u_0\rangle$ is chosen, that is associated with the site where the local density of states is calculated. It is also needed that the basis $|u_n\rangle$ is normalized and that $|u_{n-1}\rangle = 0$. Hence, the recursion relation for $n = 0$ is written as

$$H|u_0\rangle = a_0|u_0\rangle + b_1|u_1\rangle. \tag{B.2}$$

According to Eqn. B.2, it is possible to determine the coefficient a_0 by doing a scalar multiplication by $\langle u_0|$ and using the orthogonality properties, one has

$$a_0 = \langle u_0|H|u_0\rangle. \tag{B.3}$$

After a_0 is obtained, it is possible to obtain b_1 by subtracting $a_0|u_0\rangle$ in the Eqn. B.2, and then

$$b_1|u_1\rangle = (H - a_0)|u_0\rangle, \tag{B.4}$$

multiplying by its dual correspondent

$$\langle u_1 | b_1^\dagger b_1 | u_1 \rangle = \langle u_0 | (H - a_0)^\dagger (H - a_0) | u_0 \rangle , \tag{B.5}$$

using the normalization condition

$$b_1^2 = \langle u_0 | (H - a_0)^\dagger (H - a_0) | u_0 \rangle \tag{B.6}$$

or

$$b_1 = \langle u_0 | (H - a_0)^\dagger (H - a_0) | u_0 \rangle^{\frac{1}{2}} . \tag{B.7}$$

With b_1 determined, one can now calculate $|u_1\rangle$

$$|u_1\rangle = \frac{(H - a_0)}{b_1} |u_0\rangle . \tag{B.8}$$

Now, knowing a_0, b_1 and $|u_1\rangle$, one can calculate the values for a_1, b_2 and $|u_2\rangle$ analogously. Generalizing the procedure for any value of n, one can reach

$$a_n = \langle u_n | H | u_n \rangle , \tag{B.9}$$

$$b_{n+1}^2 = \left[\langle u_n | (H - a_n)^\dagger - \langle u_{n-1} | b_n^\dagger \right] \left[(H - a_n) | u_n \rangle - b_n | u_{n-1} \rangle \right] \tag{B.10}$$

and

$$|u_{n+1}\rangle = \frac{(H - a_n) | u_n \rangle - b_n | u_{n-1} \rangle}{b_{n+1}} . \tag{B.11}$$

Therefore, the Hamiltonian in its new basis can be written as

$$H_{m,n} = \langle u_m | H | u_n \rangle = \langle u_m | a_n | u_n \rangle + \langle u_m | b_{n+1} | u_{n+1} \rangle + \langle u_m | b_n | u_{n-1} \rangle \tag{B.12}$$

or

$$H_{m,n} = \langle u_m | H | u_n \rangle = a_n \delta_{m,n} + b_{n+1} \delta_{m,n+1} + b_n \delta_{m,n-1} . \tag{B.13}$$

Writing now in its matrix form

$$H = \begin{pmatrix} a_0 & b_1 & 0 & 0 & \cdots \\ b_1 & a_1 & b_2 & 0 & \cdots \\ 0 & b_2 & a_2 & b_3 & \cdots \\ 0 & 0 & b_3 & a_3 & \cdots \\ \vdots & \vdots & \vdots & \vdots & \ddots \end{pmatrix} .$$

Note that the orbitals $|u_n\rangle$ are obtained after successive applications of H on $|u_0\rangle$. Therefore, as n increases the orbitals extends itself for a big region (n+1 neighbors), therefore, the influence of orbitals $|u_{n+1}\rangle$ on $|u_0\rangle$ decreases and eventually becomes irrelevant for the local density of state calculation in this site. In the self-consistent process, the Hamiltonian transformation ends when, for a given n, $b_{n+1} = 0$ is reached. However, for a given $n > LL$ (so called cut-off parameter), the contributions of $|u_n\rangle$ are too small. Therefore, one can truncate the coefficients at $n = LL$. The value for LL is chosen given the size and complexity of the problem.

Once the new tridiagonal Hamiltonian is found, as well as the parameters a_n and b_n, one can then calculate the local density of states $N(E)$. However, the problem is truncated, therefore, the local density of states is discrete. In order to have the local density of states in the continuous spectrum, one must use a terminator to simulate the contributions of the parameters a_n and b_n with $n > LL$. These density of states are calculated using the properties of the Green function in the form of continued fraction. The local density of states for the $|u_o\rangle$ orbital can be written as

$$N_0(E) = LDOS = -\frac{1}{\pi} Im\left[G_0(E)\right], \tag{B.14}$$

where $G_0(E)$ is the first element of the principal diagonal of the matrix

$$G_0(E) = \langle u_0 | \left(E - H\right)^{-1} | u_0 \rangle, \tag{B.15}$$

being

$$\left(E-H\right)^{-1} = \begin{pmatrix} (E-a_0) & -b_1 & 0 & 0 & 0 & \cdots \\ -b_1 & (E-a_1) & -b_2 & 0 & 0 & \cdots \\ 0 & -b_2 & (E-a_2) & -b_3 & 0 & \cdots \\ 0 & 0 & -b_3 & (E-a_3) & -b_4 & \cdots \\ \vdots & \vdots & \vdots & \vdots & \vdots & \ddots \end{pmatrix}^{-1},$$

In order to obtain the elements of the inverse matrix $(E-H)$, one must calculate the ratio between the cofactor matrix and the determinant of it. Defining then $D_n(E)$ as the matrix determinant, suppressing the first n lines and columns, and $D_0(E)$ the determinant of the $(E-H)$ matrix, one can write

$$G_0(E) = \frac{D_1(E)}{D_0(E)}. \tag{B.16}$$

Using the property for determinants of a matrix $n \times n$, described by

$$detA_{n\times n} = \sum_{i=1}^{n} (-1)^{i+1} A_{i,1} D_{i,1}, \tag{B.17}$$

having that $D_{i,1}$ is the determinant of the matrix A with line i and column 1 suppressed

$$D_0(E) = (-1)^{1+1}(E-a_0)\underbrace{D_{1,1}}_{D_1(E)} + (-1)^{2+1}(-b_1)D_{2,1}, \tag{B.18}$$

with

$$D_{2,1} = (-1)^2(-b_1)D_2(E), \tag{B.19}$$

therefore,

$$D_0(E) = (E-a_0)D_1(E) - b_1^2 D_2(E). \tag{B.20}$$

Substituting these results in B.16, we have that

$$G_0(E) = \frac{D_1(E)}{D_0(E)} = \frac{D_1(E)}{(E-a_0)D_1(E) - b_1^2 D_2(E)}, \tag{B.21}$$

$$G_0(E) = \frac{1}{(E-a_0) - b_1^2 \frac{D_2(E)}{D_1(E)}}. \tag{B.22}$$

Now, notice that

$$D_1(E) = (E-a_1)(-1)^2 D_2(E) - (-b_2)^2 D_3(E). \tag{B.23}$$

In a general form, then

$$D_n(E) = (E-a_n)D_{n+1}(E) - (-b_{n+1})^2 D_{n+2}(E). \tag{B.24}$$

And finally, the $G_0(E)$ in terms of the continued fraction can be written as

$$G_0(E) = \cfrac{1}{(E-a_0) - \cfrac{b_1^2}{(E-a_1) - \cfrac{b_2^2}{(E-a_2) - \cfrac{b_3^2}{(E-a_3) - \cfrac{b_4^2}{\ddots}}}}}. \tag{B.25}$$

This continued fraction will give two different types of density of states: a discrete one, if the fraction is truncated, or a continuous if one uses the infinite fraction. As the interest of this study is the continuous limit, the fraction is truncated in the cut-off parameter and then a terminator is used to represent the missing terms. In this way, we can write

$$G_0(E) = \cfrac{1}{(E-a_0) - \cfrac{b_1^2}{(E-a_1) - \cfrac{b_2^2}{(E-a_2) - \cfrac{b_3^2}{\ddots \cfrac{}{(E-a_{LL-1}) - \cfrac{b_{LL}^2}{(E-a_{LL}) - t(E)}}}}}}, \tag{B.26}$$

where $t(E)$ is the terminator of the continued fraction and has the goal of represent the terms when $n > LL$.

Here, we will use the Beer-Pettifor terminator [53]. This terminator determines that $a_n = n$ and $b_n = n$ for the constant in $n > LL$ and the continued fraction is written as

$$t(E) = \frac{b^2}{E - a - t(E)}. \tag{B.27}$$

For $t(E)$, we have the following equation

$$[t(E)]^2 - (E-a)\,t(E) + b^2 = 0. \tag{B.28}$$

Solving this equation for $t(E)$

$$t(E) = \frac{1}{2}\left[(E-a) \pm \sqrt{(E-a-2b)\,(E-a+2b)}\right]. \tag{B.29}$$

Substituting B.29 in the continued fraction, the fraction is obtained which will generate a continuous spectrum for the local density of states in the interval

$$a - 2b < E < a + 2b. \tag{B.30}$$

Finally, one can calculate the total local density of states if one sums up all the contributions coming from each orbital for a given site.

Appendix C.
Multiple scattering theory

The multiple scattering theory (MST) is a mathematical formalism that is useful when describing the propagation of a wave through different scatters. The MST is widely use in several areas of physics and particularly here, in condensed matter, the formalism becomes handy when dealing with electronic structure calculations. In our case, it will be use to describe the interactions between two magnetic moments. Interactions explored in this thesis, such as the exchange-coupling and the Dzyaloshinskii-Moriya interactions, were mathematically described by the MST and further developed into the LMTO language. For more detailed information about the MST, one should take a look at the notes in Ref. [73].

C.1 Grand canonical potential from the integrated DOS

A good and convenient way to determine the electronic structure of a given system is to work within the grand canonical potential. The grand canonical ensemble states that the energy and particles of a system can be changed with a reservoir, i.e. the chemical potential μ and the absolute temperature T are the thermodynamic variables. The grand canonical potential can be written as

$$\mathscr{E} = \int_{-\infty}^{\infty} d\varepsilon \varepsilon f(\varepsilon) n(\varepsilon) \tag{C.1}$$

and N is the (average) number of particles given by the equation

$$N = \int_{-\infty}^{\infty} d\varepsilon f(\varepsilon) n(\varepsilon) \,, \tag{C.2}$$

where $f(\varepsilon) = 1/\left(1 + e^{\beta(\varepsilon-\mu)}\right)$ is the Fermi-Dirac distribution function parametrized with the inverse temperature $\beta = 1/(k_B T)$. The $n(\varepsilon)$ stands for the density of states (DOS) as a function of the energy variable ε. Considering that the Fermi-temperature is usually much higher than the critical (Curie) temperature, it is enough to work in the $T = 0$ approach when the energy integration goes up to ε_F (and $f(\varepsilon)$ is a step function). In this case

$$\Omega = \mathscr{E} - \varepsilon_F N = \int_{-\infty}^{\varepsilon_F} d\varepsilon \varepsilon n(\varepsilon) - \varepsilon_F N \,, \tag{C.3}$$

or

$$\Omega = \varepsilon_F N(\varepsilon_F) - \int_{-\infty}^{\varepsilon_F} d\varepsilon N(\varepsilon) - \varepsilon_F N \,, \tag{C.4}$$

where $N(\varepsilon)$ is the integrated DOS (IDOS) that was obtained through a partial integration in Eqn. C.3. Considering that $N(\varepsilon_F) = N$, it is possible to verify that the first and third term cancel each other in Eqn. C.4. Therefore, the grand canonical potential can be written as

$$\Omega = -\int_{-\infty}^{\varepsilon_F} d\varepsilon N(\varepsilon) \,. \tag{C.5}$$

This means that one is able to determine the variations of the IDOS to get the variations of the grand potential. For this purpose we will derive the Lloyd formula after introducing the needed MST quantities.

C.2 Green function and DOS

Particularly in the electronic structure field, the Green function gives us the information about how an electron in a site *i* interacts with an electron in site *j* or vice-versa. This information is extremely valuable when calculating interactions between two atoms, such as the exchange interactions explored in this thesis. This particular form of Green function is called inter-site Green function. Other particular form of the Green function, so called intra-site Green function, will gives us the information within the atom in the site *i* and it gives us each orbital occupation. Here, the Green function will be discussed and its interpretation in the electronic structure. The Green function of a given Hamiltonian H is defined as

$$G(z) = (z - H)^{-1} \,, \tag{C.6}$$

where $z \in \mathbb{C}$. It implies that $G(z^*) = G^{\dagger}(z)$. If both sides of the equation

$$(z_2 - H) - (z_1 - H) = z_2 - z_1 \tag{C.7}$$

are multiplied by $G(z_1)G(z_2)$ then the equation

$$(z_1 - H)^{-1} - (z_2 - H)^{-1} = (z_2 - z_1)(z_1 - H)^{-1}(z_2 - H)^{-1} \,, \tag{C.8}$$

is obtained. Assuming that $z_2 = z + dz$, $z_1 = z$ and $dz \to 0$, the equation

$$\frac{dG(z)}{dz} = -G^2(z) \; . \tag{C.9}$$

can be derived.

Let us now assume that the Hamiltonian H has a discrete spectrum (the conclusions can be extended to the continuous spectrum), i.e. $H\varphi_n = \varepsilon_n \varphi_n$. Then the spectral resolution of the Green function (Lehmann representation) can be obtained as

$$G(z) = \sum_n \frac{|\varphi_n\rangle\langle\varphi_n|}{z - \varepsilon_n} \; . \tag{C.10}$$

It implies firstly that on the basis of the eigenfunction of H the Green function would be represented as $G_{nn'}(z) = \delta_{nn'} \frac{1}{z-\varepsilon_n}$. Secondly, the $G(z)$ is obviously undefined for a $z = \varepsilon_n$. However, we can define the up and down side limits of $G(z)$ as the following

$$G^{\pm}(\varepsilon) = \lim_{\delta \to 0} G(\varepsilon \pm i\delta) \; . \tag{C.11}$$

Note that $G^{\pm}(\varepsilon) = (G^{\mp}(\varepsilon))^{\dagger}$. The notation defined by Eqn. C.11 will be later used for the T-matrix.

In a system of independent fermions, the measured value of a one-particle observable, A, is given as

$$\overline{A} = \sum_n p_n \langle\varphi_n|A|\varphi_n\rangle \; , \tag{C.12}$$

where $p_n = f(\varepsilon_n)$, and Fermi-Dirac distribution function $f(\varepsilon)$ has been introduced already.

Using the Cauchy's theorem, which states that for a closed contour clockwise oriented, the integration of the equation $g(z)/(z-a)$ is equal to $-2\pi i g(a)$ if a is within the contour and 0 if a is outside. We should keep in mind that the Fermi-Dirac function $f(z)$ also has Matsubara poles. However, if the contour is performed on the real axis then, with the help of the Cauchy's theorem and Eqn. C.10, the Eqn. C.12 can be simply given by $G^+(\varepsilon)$ as the following

$$\overline{A} = -\frac{1}{\pi} \Im \int_{-\infty}^{\infty} d\varepsilon f(\varepsilon) Tr\left(A G^+(\varepsilon)\right) \; . \tag{C.13}$$

If A is the identity operator then it can be written that

$$N = -\frac{1}{\pi} \Im \int_{-\infty}^{\infty} d\varepsilon f(\varepsilon) Tr\left(G^+(\varepsilon)\right) \; . \tag{C.14}$$

Comparing Eqn. C.2 with Eqn. C.14, it can be obtained for the DOS that

$$n(\varepsilon) = -\frac{1}{\pi} \Im Tr\left(G^+(\varepsilon)\right) \; . \tag{C.15}$$

C.3 T-operator and Lloyd formula

If one considers the unperturbed Hamiltonian H_0 and the operator V as a perturbation, the perturbed system can be written as

$$H = H_0 + V \ . \tag{C.16}$$

The Green function for the unperturbed and perturbed system is given as $G_0(z) = (z - H_0)^{-1}$ and $G(z) = (z - H)^{-1}$, respectively. Then it can be written that

$$G(z) = (z - H_0 - V)^{-1} = [(z - H_0)(I - G_0(z)V)]^{-1} \ , \tag{C.17}$$

where I is the identity operator. For the Green function we can write a Dyson equation as $G(z) = G_0(z) + G_0(z)VG_0(z) + G_0(z)VG_0(z)VG_0(z) + \dots$. Introducing the T-operator,

$$T(z) \equiv V + VG_0(z)V + VG_0(z)VG_0(z)V + \dots \ , \tag{C.18}$$

the perturbed Green function can then be written as

$$G(z) = G_0(z) + G_0(z)T(z)G_0(z) \ . \tag{C.19}$$

It follows from the definition of $T(z)$ that $T(z) = V + VG(z)V$. It can be shown that

$$G_0(z)T(z) = G(z)V \qquad\qquad T(z)G_0(z) = VG(z) \ . \tag{C.20}$$

These expressions imply that

$$T(z) = V + VG_0(z)T(z) \ . \tag{C.21}$$

Considering that $T(z) = V + VG(z)V$, the derivative of $T(z)$ with respect to z is $V\frac{dG(z)}{z}V$. Using Eqns. C.9 and C.20, we can write for the derivative of $T(z)$ that

$$\frac{T(z)}{dz} = T(z)\frac{dG_0(z)}{dz}T(z) \ . \tag{C.22}$$

The Eqn. C.15 tells us how to calculate the DOS. For the perturbed DOS it can be written that

$$n(\varepsilon) = -\frac{1}{\pi}\Im Tr\left(G^+(\varepsilon)\right) = -\frac{1}{\pi}\Im Tr\left(G_0^+(\varepsilon) + G_0^+(\varepsilon)T^+(\varepsilon)G_0^+(\varepsilon)\right) \tag{C.23}$$

by using of Eqn. C.19. Introducing the unperturbed DOS as $n_0(\varepsilon) = -\frac{1}{\pi}\Im Tr\left(G_0^+(\varepsilon)\right)$, the perturbed DOS can be written as $n(\varepsilon) = n_0(\varepsilon) + \delta n(\varepsilon)$ where

$$\delta n(\varepsilon) = -\frac{1}{\pi}\Im Tr\left(G_0^+(\varepsilon)T^+(\varepsilon)G_0^+(\varepsilon)\right) = -\frac{1}{\pi}\Im Tr\left(\left(G_0^+\right)^2(\varepsilon)T^+(\varepsilon)\right) . \tag{C.24}$$

We used the cyclic property of the trace in the last step. For $\left(G_0^+\right)^2$ using Eqn. C.9 we get that

$$\delta n(\varepsilon) = \frac{1}{\pi}\Im Tr\left(\frac{G_0^+(\varepsilon)}{d\varepsilon}T^+(\varepsilon)\right) = \frac{1}{\pi}\Im Tr\left(\left(T^+(\varepsilon)\right)^{-1}T^+(\varepsilon)\frac{G_0^+(\varepsilon)}{d\varepsilon}T^+(\varepsilon)\right) , \tag{C.25}$$

where we inserted the identity $\left(T^+(\varepsilon)\right)^{-1}T^+(\varepsilon)$ in the last step. The Eqn. C.22 simplifies the variation of the DOS as follows

$$\delta n(\varepsilon) = \frac{1}{\pi}\Im Tr\left(\left(T^+(\varepsilon)\right)^{-1}\frac{T^+(\varepsilon)}{d\varepsilon}\right) , \tag{C.26}$$

which can be further formulated as

$$\delta n(\varepsilon) = \frac{d}{d\varepsilon}\frac{1}{\pi}\Im Tr\ln\left(T^+(\varepsilon)\right) . \tag{C.27}$$

If the variation of the DOS is given as an energy derivative then for the variation of the IDOS can be written that

$$\delta N(\varepsilon) = \frac{1}{\pi}\Im Tr\ln\left(T^+(\varepsilon)\right) . \tag{C.28}$$

We have derived the so-called Lloyd formula which tells us how to get the variation of the IDOS due to a representation of the T-operator.

C.4 Fundamental equation of MST

Next, we specify what the operator V stands for. It can be written as a sum of single-domain potential, i.e.

$$V = \sum_i V_i , \tag{C.29}$$

where V_i is the single site potential at site i. This can be a single muffin-tin potential which is described by a spherical symmetric potential within a radius of an atomic position, and equals to a constant (muffin-tin zero) outside the radius. In general, the corresponding *single site scattering operator* can be written as

$$t_i(\varepsilon) = V_i + V_i G_0(\varepsilon) t_i , \tag{C.30}$$

see Eqn. C.21. Note that the up-side energy limit will be considered, see Eqn. C.11 for a definition, however, the + symbol will be not written. Inserting Eqn. C.29 into Eqn. C.18 leads to the relation

$$T = \sum_{ij} \tau_{ij} \,, \tag{C.31}$$

where the scattering path operator (SPO)

$$\tau_{ij} = t_i \delta_{ij} + t_j G_0 (1 - \delta_{ij}) t_j + \sum_k t_i G_0 (1 - \delta_{ik}) t_k G_0 (1 - \delta_{km}) t_m + \ldots \tag{C.32}$$

has been introduced. In order to simplify the following steps, the energy variable, ε, is dropped in Eqns. C.31 and C.32. Next, we introduce the notation $\tau(\varepsilon)$ and $\mathbf{t}(\varepsilon)$ as the set of the $\{\tau_{ij}(\varepsilon)\}$ and $\{t_i(\varepsilon)\}$ matrices, respectively. Using Eqns. C.30 and C.32, we can formulate the fundamental (Dyson) equation of the multiple scattering theory as the following

$$\tau(\varepsilon) = \left(\mathbf{P}(\varepsilon) - \mathbf{G}_0(\varepsilon)\right)^{-1} \,, \tag{C.33}$$

where

$$\mathbf{P}(\varepsilon) = \mathbf{t}^{-1}(\varepsilon) \equiv \left\{P_i(\varepsilon)\,\delta_{ij}\right\} = \left\{t_i^{-1}(\varepsilon)\,\delta_{ij}\right\} \tag{C.34}$$

the inverse of single site scattering operator (ISO) while $\mathbf{G}_0(\varepsilon) = \left\{G_{0,ij}(\varepsilon)\,(1-\delta_{ij})\right\}$ stands for the Green function of the free system (which is called as structure constant).

References

[1] R. Wiesendanger, Rev. Mod. Phys. 81, 1495 (2009).
[2] D. Serrate *et al.*, Nature Nanotech. 5, 350 (2010).
[3] F. Meier *et al*., Science 320, 82 (2008).
[4] L. Zhou *et al*., Nature Physics 6, 187 (2010).
[5] M. Bode *et al*., Nature 447, 190 (2007).
[6] M. Bode *et al*., Nature Mater. 5, 477 (2006).
[7] C. L. Gao *et al*., Phys. Rev. Lett. 98, 107203 (2007).
[8] C. L. Gao *et al*., Phys. Rev. Lett. 100, 237203 (2008).
[9] D. Wortmann *et al*., Phys. Rev. Lett. 86, 4132 (2001).
[10] C. L. Gao, W. Wulfhekel, and J. Kirschner, Phys. Rev. Lett. 101, 267205 (2008).
[11] T. Jamneala, V. Madhavan, and M. F. Crommie, Phys. Rev. Lett. 87, 256804 (2001).
[12] P. Wahl *et al*., Phys. Rev. Lett. 98, 056601 (2007).
[13] G. Binnig, C. F. Quate, and Ch. Gerber, Phys. Rev. Lett. 56, 930 (1986).
[14] M. Born and J. R. Oppenheimer, Ann. der Phys. 84, 457 (1927).
[15] M. Born and K. Huang. *Dynamical Theory of Crystal Lattices*. Oxford University Press, New York (1954).
[16] P. Hohenberg and W. Kohn, Phys. Rev. 136, B 864 (1964).
[17] W. Kohn and L. J. Sham, Phys. Rev. 140, A1133 (1965).
[18] S. Frota-Pessôa, Phys. Rev. B 46, 22 (1992).
[19] A. B. Klautau and S. Frota-Pessôa, Surf. Sci. 579, 27-36 (2005).
[20] A. Bergman *et al*., Phys. Rev. B 73, 174434 (2006).
[21] A. Bergman *et.al*., Phys. Rev. B 75 224425 (2007).
[22] I. Dzyaloshinskii, J. Phys. and Chem. of Solids 4, 241 (1958).
[23] T. Moriya, Phys. Rev. 120, 91 (1960).
[24] B. Skubic *et al.*, J. Phys. Condens. Matter, 20, 315203 (2008).
[25] H. Nyquist, Phys. Rev. 32, 110 (1928).
[26] K. Binder and D. P. Landau. *Introduction to modern statistical mechanics*. Oxford University Press, Oxford (1987).
[27] S. Paul *et al*., Phys. Rev. B 97, 125120 (2018).
[28] P. Söderlind *et al*., Phys. Rev. B 96, 100404(R) (2017).
[29] R. Chimata *et al*., Phys. Rev. B 95, 214417 (2017).
[30] S. Keshavarz *et al*., Phys. Rev. B 95, 115120 (2017).
[31] I. L. M. Locht *et al*., Phys. Rev. B 94, 085137 (2016).
[32] R. Yadav *et al*., `arXiv:1707.00500 [cond-mat.str-el]`
[33] K. Koumpouras *et al*., `arXiv:1702.00579 [cond-mat.mes-hall]`
[34] S. Heinze *et al*., Nat. Phys. 7, 713 (2011).
[35] M. Pereiro *et al*., Nat. Commun. 5, 4815 (2014).
[36] A. Fert, N. Reyren, and V. Cros, Nat. Rev. Materials, 2, 17031 (2017).

[37] S. Hoshino and N. Nagaosa, Phys. Rev. B 97, 024413 (2018).
[38] Y. Zhang *et al*., Nanoscale, 9, 10212-10218 (2017)
[39] D. Maccariello *et al*., Nat. Nanotech., 13, 233-237 (2018).
[40] M. H. Seaberg *et al*., Phys. Rev. Lett. 119, 067403 (2017).
[41] T. Matsumoto *et al*., Nano Lett. 18, 2, 754-762 (2018).
[42] M. B. A. Jalil *et al*., J. of Magn. Magn. Mater. 399, 155-158 (2016).
[43] L. J. Sham and W. Kohn, Phys. Rev. 145, 561 (1966).
[44] U. von Barth and L. A. Hedin, J. Phys. C 5, 1629 (1972).
[45] O. K. Andersen, Phys. Rev. B 12, 3060 (1975).
[46] D. D. Koelling and B. N. Harmon, J. Phys. C 10, 3107 (1977).
[47] M. S. S. Brooks and P. J. Kelly, Phys. Rev. Lett. 51, 1708 (1983).
[48] J. Kübler. *Theory of Itinerant Electron Magnetism*. Oxford University Press, New York (2000).
[49] S. Blundell. *Magnetism in Condensed Matter*. Oxford University Press, New York (2001).
[50] O. K. Andersen and O. Jepsen, Phys. Rev. Lett. 53, 27 (1984).
[51] O. K. Andersen, O. Jepsen, and D. Glötzel, *Highlights of condensed matter theory*. North Holland, Amsterdam (1985).
[52] R. Haydock, *Solid State Physics*, vol.35. Academic Press, New York (1980); R. Haydock, V. Heine, and M. J. Kelly, J. Phys. C 8, 2591 (1975).
[53] N. Beer and D. G. Pettifor, *The Electronic Structure of Complex Systems*. Plenum Press, New York (1984).
[54] H. L. Skriver and N. M. Rosengaard, Phys. Rev. B 43, 9538 (1991).
[55] M. Aldén *et al*., Phys. Rev. B 46, 6303 (1992).
[56] A. Bergman *et al*., Phys. Rev. B 75, 224425 (2007).
[57] A. Bergman *et al*., Surf. Sci. 600, 4838 (2006).
[58] Munich SPR-KKR band structure program package: http://ebert.cup.uni-muenchen.de.
[59] A. I. Liechtenstein *et al*., J. Magn. Magn. Mater. 67, 65 (1987).
[60] S. Frota-Pessôa, R. B. Muniz, and J. Kudrnovský, Phys. Rev. B 62, 5293 (2000).
[61] M. van Schilfgaarde and V. P. Antropov, J. Appl. Phys. 85, 4827 (1999).
[62] O. K. Andersen, O. Jepsen, and M. Sob, *Linearized Band Structure Methods*. Springer, New York (1987).
[63] A. Szilva *et al*., Phys. Rev. Lett. 111, 127204 (2013).
[64] A. Deák, *Dzyaloshinsky-Moriya interaction in metals*, BSc dissertation. Department of Theoretical Physics, Institute of Physics, Budapest University of Technology and Economics (2009).
[65] S. Lounis and P. H. Dederichs, Phys. Rev. B 82, 180404(R) (2010).
[66] A. Szilva *et al*., Phys. Rev. B 96, 144413 (2017).
[67] V. P. Antropov, B.N. Harmon and A.N. Smirnov, J. Magn. Magn. Mater. 200, 148-166 (1999).
[68] L. Udvardi and L. Szunyogh Phys. Rev. Lett. 102, 207204 (2009).
[69] A. Antal *et al*., Phys. Rev. B 77, 174429 (2008).
[70] M. dos Santos Dias *et al*., Nature Communications 7, 13613 (2016).
[71] T. Kikuchi *et al*., Phys. Rev. Lett. 116, 247201 (2016).
[72] A. B. Klautau, *Cálculos Ab Initio da Estrutura Eletrônica e Propriedades*

Magnéticas de Sistemas Metálicos Bidimensionais PhD Thesis, Universidade de São Paulo, Brasil (2000).
[73] Retrieved from http://newton.phy.bme.hu/ szunyogh/Elszerk/Kkr-slides.pdf.
[74] F. Freimuth *et al*., Phys. Rev. B 96, 054403 (2017).

Acta Universitatis Upsaliensis

Digital Comprehensive Summaries of Uppsala Dissertations from the Faculty of Science and Technology 1663

Editor: The Dean of the Faculty of Science and Technology

A doctoral dissertation from the Faculty of Science and Technology, Uppsala University, is usually a summary of a number of papers. A few copies of the complete dissertation are kept at major Swedish research libraries, while the summary alone is distributed internationally through the series Digital Comprehensive Summaries of Uppsala Dissertations from the Faculty of Science and Technology. (Prior to January, 2005, the series was published under the title "Comprehensive Summaries of Uppsala Dissertations from the Faculty of Science and Technology".)

Distribution: publications.uu.se
urn:nbn:se:uu:diva-347812

ACTA
UNIVERSITATIS
UPSALIENSIS
UPPSALA
2018